Machine learning thermobarometry and chemometry using amphibole and clinopyroxene: a window into the roots of an arc volcano (Mount Liamuiga, Saint Kitts)

Oliver Higgins[1]*, Tom Sheldrake[1], Luca Caricchi[1]

[1]Department of Earth Sciences, University of Geneva, rue des Maraîchers 13, 1205, Geneva, Switzerland

*Corresponding author (oliver.higgins@unige.ch; ORCID iD: 0000-0001-9960-934X)

T.S ORCID iD: 0000-0002-7192-4273

L.C ORCID iD: 0000-0001-9051-2621

Social Media Affiliations

@MAGEvolcano @4ohiggins4 @NatHazTom @LucaCaricchi

Keywords

single-phase; Mansion Series; anorthite; stratigraphy; compositional gap

Funding

O. H., T.S and L. C. received funding from the European Research Council (ERC) under the European Union's Horizon 2020 research and innovation program (Grant agreement 677493 - FEVER). TS was also supported by funding from SNSF (GEOVOLCO - PCEFP2_194204).

Abstract

The physical and chemical properties of magma govern the eruptive style and behaviour of volcanoes. Many of these parameters are linked to the storage pressure and temperature of the erupted magma, and melt chemistry. However, reliable single-phase thermobarometers and chemometers which can recover this information, particularly using amphibole chemistry, remain elusive. We present a suite of single-phase amphibole and clinopyroxene thermobarometers and chemometers, calibrated using machine learning. This approach allows us to intimately track the range of pre-eruptive conditions over the course of a millennial eruptive cycle on an island arc volcano (Saint Kitts, Eastern Caribbean). We unpick the story of Mount Liamuiga, a stratovolcano that pops its upper-crustal (2 kbar), dacitic cork at the beginning of the Lower Mansion Series eruptive sequence. This permits a progressive increase in the thermal maturity of the magma arriving at the surface from the middle to upper crust (2 – 5.5 kbar) through time. The temperature increase correlates well with matrix plagioclase chemistry, which itself displays a remarkable progression to less evolved (more anorthitic) composition in time. We find that amphibole is a reliable themobarometer (SEE = 1.4 kbar; 40 ˚C), at odds with previous studies. We suggest it is the regression strategy, as opposed to the abject insensitivity to pressure, that has hindered previous calibrations of amphibole only thermobarometers. By recognising this, we have constructed a high-resolution, quantitative picture of the magma plumbing system beneath an arc volcano.

Introduction

Accurately recording the pressure and temperature distribution of magma storage is critical for our understanding of volcanic igneous plumbing systems (Blundy and Cashman, 2008). This includes the ability to compare the pressure and temperature of erupted products with monitoring signals to quantitatively link eruption size, explosivity and duration (eruptive dynamics) to pre-eruptive magma storage conditions (Voight, 1988). Assessing such parameters temporally, be it relative time in the form of stratigraphy (Sisson and Vallance, 2009) or absolute time from crystal ages (e.g. Shane, 2013), may improve our understanding of how, why and when these dynamics change during an eruptive cycle (Ridolfi et al., 2008; Shane, 2013).

Determinations of intensive parameters (pressure, temperature, melt composition; P, T, X) for a magma can be made using the results of equilibrium experiments, run at specific conditions to match mineral and melt chemistry of erupted products (Pichavant et al., 2007; Sisson et al., 2005; Solaro et al., 2019). Additionally, a thermometer (T), barometer (P), or chemometer (X) that relates mineral phase chemistry to known pressure, temperature, and melt composition can be calibrated (Blundy and Cashman, 2008; Putirka, 2008). Statistical relationships are derived using an array of approaches: linear regression (Ridolfi et al., 2008; Ridolfi and Renzulli, 2012); direct correlation with unit cell parameters (Nimis, 1995; Nimis and Ulmer, 1998); multiphase reaction barometry (P_{av} method; Ziberna et al., 2017); linear least-square regression with a thermodynamic basis (Putirka, 2008); machine learning (this study; Petrelli et al., 2020; Jorgenson et al., 2021).

Amphibole and clinopyroxene are phases commonly used as thermobarometers. Clinopyroxene is typically coupled with melt for thermobarometry (Neave and Putirka, 2017; Putirka, 2016, 2008). The caveat is that an equilibrium melt requires matrix glass (for crystal rims) or melt inclusions (for crystal cores/ mantles). Whilst solutions, such as calculating liquids using mass balance (Hammer et al., 2016) or iterative melt matching schemes (Neave et al., 2019), have been proposed, the associated uncertainty of matching a melt with a mineral is rarely propagated. Without an equilibrium melt, an independent estimate of temperature is required (Nimis and Ulmer, 1998) which introduces further uncertainty. Amphibole has enormous potential for pressure and temperature determinations due to its common occurrence in hydrous arc magmas (Scaillet and Evans, 1999) and compositional diversity (Leake et al., 1997). Temperature estimates may be obtained from amphibole – plagioclase (Blundy and Holland, 1990; Holland and Blundy, 1994), amphibole – melt (Putirka, 2016), and in some cases, amphibole only (Erdmann et al., 2014; Ridolfi and Renzulli, 2012; Shane, 2013). Amphibole has also been successfully calibrated as a chemometer, notably for prediction of equilibrium melt SiO_2 (Zhang et al., 2017).

However, its use as a reliable barometer is debated. It is best applied in multiply-saturated granitic systems (T < 800 ˚C; Fe# < 0.65; Anderson and Smith, 1995; Putirka, 2016) whereas calibrations of amphibole-only barometers (e.g. Ridolfi and Renzulli, 2012) have been widely criticised (Erdmann et al., 2014; Putirka, 2016; Shane, 2013). Additionally, errors from amphibole barometry are consistently quoted at ±3 – 4 kbar which approaches the edge of usability for identifying the loci of pre-eruptive magma storage (Putirka, 2016).

The Eastern Caribbean (Lesser Antilles) island arc has been an area of recent interest to determine crustal structure (Kopp et al., 2011), water flux (Cooper et al., 2020), and the structure of sub-volcanic systems (Melekhova et al., 2019). This is due to its reputation for both significant volcanic hazards (Lindsay, 2005) and as an exemplar of a slow subduction zone (Wadge and Shepherd, 1984). Particular attention has been paid to constraining the sub-volcanic crustal structure using magmatic inclusions (widely referred to as “plutonics”, “cumulates” or “xenoliths”) along the arc by employing experimental petrology (Melekhova et al., 2017, 2015; Stamper et al., 2014), thermodynamic modelling (Stamper et al., 2014), and a host of thermobarometers (Camejo-Harry et al., 2018). Nonetheless, these inclusions are largely found ex situ (Arculus and Wills, 1980) and so lack temporal (with regards to the eruption) or spatial (with regards to the eruptive centre) information. In contrast, the excellent exposure of fall and flow deposits in the Eastern Caribbean (Baker and Holland, 1973; Howe et al., 2014) provides a preferable record of time-integrated P-T-X which may be linked to evolving conditions in the sub-volcanic system. However, natural fragmentation in pyroclastic rocks (e.g. Higgins et al., 2021) and compositional diversity in silicate phases at thin-section scale (notably plagioclase; Toothill et al., 2007) precludes the use of thermobarometers based on equilibrium pairs (Shane, 2013). In addition, suitable single-phase thermobarometers applicable to a range of melt compositions are lacking.

We present a suite of new thermobarometers and chemometers (amphibole-only and clinopyroxene-only), calibrated using machine learning. This approach has proved successful for clinopyroxene thermobarometry applied to alkalic magmas from Iceland (Petrelli et al., 2020). We use a section of the Mansion Series stratigraphy (Baker, 1969; Roobol et al., 1981; Higgins et al., 2021) on the island of Saint Kitts, Eastern Caribbean, to temporally track the variation of intensive parameters in pyroclastic samples. These are then linked to the remarkably clear increase of matrix plagioclase anorthite content (An#) in time for the same sequence (Higgins et al., 2021). Where possible, we corroborate the P-T-X results with evidence from geochemistry, petrography, and textural observations. The development of such reliable single-phase thermobarometers and chemometers is critical for the wider volcanology community as they provide a quantitative metric to cross-compare volcanic systems and their dynamic behaviours, a notoriously difficult task in Earth sciences (Cashman and Biggs, 2014).

Geological Setting

Saint Kitts (**Fig. 1a**) is a northern island in the Eastern Caribbean island arc, resulting from the slow (2 – 4 cm/year; Shepherd, 1984), westward subduction of the North American plate beneath the Caribbean plate. Recent volcanism on Saint Kitts (~ 42 ka; Roobol et al., 1981) originates from the Mount Liamuiga stratovolcano in the north west, depositing the Mansion Series stratigraphy (Baker, 1969; Roobol et al., 1981; **Fig.1a**). The Mansion Series consists of 6 main units (A – F; Roobol et al., 1981). The older Lower Mansion Series, the focus of this study, comprise the Lower Green Lapilli (A), Cinder Unit (B), and Upper Green Lapilli (C). The Green Lapilli layers are primarily grey-green, angular, aphyric, micro-vesicular lapilli of andesitic composition, a rock type not noted elsewhere in the Eastern Caribbean. The eruptive sequence resumes at 4270 BP ± 140 until 2070 ± 150 (Baker, 1985) with units D – F. They are composed of interbedded ash, pumice fall deposits and pyroclastic flow deposits, along with intercalations of the Steel Dust Series fall deposits on the western flanks of Mount Liamuiga. Pyroclastic flow deposits, restricted to the north and west of Mount Liamuiga, are morphologically divided into bimodal andesitic block and ash flows and polymodal basaltic-andesite block and ash flows (Tate and Wilson, 1988). The excellent exposure of the Saint Kitts stratigraphy has inspired several studies of chemical and physical changes in the volcanic deposits through time (Baker, 1980; Baker and Holland, 1973; Higgins et al., 2021).

Methods

Fieldwork and sample preparation

Samples were collected from a 6.8 m thick, stratigraphic section on the east coast of Saint Kitts (**Fig. 1b**; 17.38725, -62.76276 [WGS84]; midway between the villages of Mansion and Tabernacle; Higgins et al., 2021; Sheldrake and Higgins, 2021). This section includes the "Pre-Mansion Series pyroclastic deposits" (> 43000 BP) and Mansion Series units A – C (> 41420 to > 41730 BP) which have been dated using ^{14}C (Harkness et al., 1994; Roobol et al., 1981). Juvenile material (pumice, mafic scoria or volcanic ash) was collected for chemical analysis, and thicknesses of volcanic units and palaeosoils measured. Beds were sampled at changes in deposit form or macroscopic mineralogy to capture the full variability of the sequence. Samples selected for thermobarometry and chemometry were those which contained phenocrysts of amphibole or clinopyroxene. Data were also included from two in-situ enclaves: one mafic enclave in SK392 (olivine + plagioclase + clinopyroxene + orthopyroxene

+ spinel) and one felsic enclave in SK386B (plagioclase + amphibole + quartz + Fe-oxide). For a more detailed appraisal of the sequence and whole rock textures refer to Higgins et al (2021).

Electron Probe Micro-analyser (EPMA)

In-situ mineral analyses of amphibole and clinopyroxene were made on 30 μm polished thin sections using a JEOL 8200 Superprobe at the University of Geneva and a JEOL JXA-8530F at the University of Lausanne. Both microprobes were equipped with a five-channel wavelength-dispersive spectroscope system (WDS) and were operated at an accelerating voltage of 15 keV, a beam current of 20 nA, and a beam diameter of 3 μm. Quantitative analyses were made using internal standards (orthoclase [Si, K], andalusite [Al], albite [Na], forsterite [Mg], fayalite [Fe], wollastonite [Ca], Mn-Ti-oxide [Mn, Ti], Cr-oxide [Cr]). Mineral analyses were acquired as transects or points to capture chemical variability within the mineral phase.

Machine learning thermobarometry

Experimental data for the calibration of two new single-phase thermobarometers (clinopyroxene-only and amphibole-only) were collected from the Library of Experimental Phase Relations (LEPR) database (Hirschmann et al., 2008) and supplemented with experiments from the geological literature (**Supplementary Table 1)**. Data spanned 0.002 kbar to 12 kbar and 750 – 1250˚C, covering the crustal thickness (Kopp et al., 2011; Melekhova et al., 2019) and inferred range of magmatic temperatures (Melekhova et al., 2017; Toothill et al., 2007) beneath Saint Kitts. Experiments at 1 atmosphere (clinopyroxene) were excluded as they tend to exhibit an anomalously wide range of Al contents. This has been ascribed to Na-loss during the experiment (Putirka, 2008) or coupled substitution of Na and Al for Si, Ca and Mg in fast growing, disequilibrium clinopyroxene at low pressure (Mollo et al., 2010; Ziberna et al., 2017). Binary cation plots for all calibrant experiments are shown in **Supplementary Fig. 1**.

Major element cations in amphibole and clinopyroxene were calculated for all experiments on the basis of 6 (clinopyroxene) and 23 (amphibole) oxygens according to Deer et al (1997). In both cases all Fe was assumed as ferrous, as per Putirka (2016), as spectroscopic analysis of Fe speciation shows that stoichiometric Fe has little correlation to measured values (Al'meev et al., 2002; Dyar et al., 1993, 1992; Hawthorne and Oberti, 2007). Poor quality analyses were filtered on the basis of cation sums for amphibole ($15 < \text{cation sum} < 16$) and clinopyroxene ($3.95 > \text{cation sum} > 4.05$). Clinopyroxene was further screened using the partition coefficient of Fe and Mg between liquid and crystal [$K_D(Fe\text{-}Mg)^{cpx\text{-}liq}$], removing values that did not fall between 0.04 and 0.68 (Putirka, 2008). Any experiments that did not report a coexisting liquid were excluded.

The final filtered datasets (n = 391 for amphibole; n = 676 for clinopyroxene) were used to train regression models with the extraTrees (v 1.0.5) package (Simm et al., 2014) in R (Team, 2013). The extraTrees package encompasses a machine learning method for classification and regression, employing a series of uncorrelated decision trees to reach a prediction output based on an input. An example of a single decision tree for temperature prediction in amphibole is found in **Supplementary Fig. 2.** The experimental composition of the amphibole (Si, Al, Ti, Ca, Na, K, Fe, Mg, Mn) / clinopyroxene (Si, Al, Ti, Ca, Na, Fe, Mg, Mn, Cr) was the input, and the experimental pressure and temperature was the output. The experimental dataset was split into a train dataset (used to train the model by correlating compositional changes in minerals with known pressures and temperatures), and a test dataset (used to verify the models' performance by predicting pressure and temperature based on composition and calculating a residual to the known experimental value). Those experiments in the test dataset are never present in the train dataset. Hyperparameter tuning is shown to have little effect on uncertainty or precision of machine learning thermobarometers (Petrelli et al., 2020; Jorgenson et al., 2021) and so we take the values of 300 trees and 6 features per node (mtry = 6). For a more extensive review of machine learning thermobarometry refer to Jorgenson et al (2021).

Petrological experiments are more commonly performed at lower pressure (2 kbar), with barometric gaps at 9 and 11 kbar. High-pressure experiments are also typically performed at higher temperature (**Fig. 2**). Therefore, we used a uniform pressure-temperature grid when sampling the test dataset, whereby a single random experiment was sampled from within each grid square. This ensured a uniform and representative pressure-temperature distribution in the test dataset. To gauge the effect of sampling certain experiments in different test and train datasets we randomly resampled both datasets 200 times (r = 200) and repeated the model calibration. The performance of the model was determined using a standard error estimate (SEE; **Eq. 1**) and a root mean square error (R^2; **Eq. 2**) based on the ability of the algorithm to predict the test (unknown) dataset. For brevity, amphibole and clinopyroxene thermobarometers will be shortened to TB(A) and TB(C) respectively.

$$R^2 = 1 - \frac{\sum_{i=1}^{n}(y_i - \hat{y}_i)^2}{\sum_{i=1}^{n}(y_i - \bar{y}_i)^2} \tag{1}$$

$$SEE = \sqrt{\frac{\sum_{i=1}^{n}(y_i - \hat{y}_i)^2}{n}} \tag{2}$$

Machine learning chemometry

A series of clinopyroxene only and amphibole only chemometers were calibrated to predict the chemistry of the coexisting melt (SiO_2, Al_2O_3, CaO, Na_2O, K_2O, MgO, FeO) with amphibole/clinopyroxene. The calibration strategy, including the experimental datasets, were identical to those used for the thermobarometers. The exception was that temperature (˚C) for the experiments was used as an additional predictor variable as this significantly reduced the SEE. Hence, when the chemometers are applied to natural minerals, we use the associated temperature from the machine learning thermometer as a predictor along with the mineral chemistry. The SEEs of each chemometer are reported in **Supplementary Table 2**.

Equilibrium experiment matching

A common approach to determine pre-eruptive storage conditions of magma is to compare the results of equilibrium experiments with natural mineral chemistry (e.g. Pichavant and Macdonald, 2007). Mismatch may arise due to experimental gaps (such as the lack of experiments at certain pressures; **Fig. 2**) or additional processes (mixing, resorption). To synthesise this approach we used a custom search script written in R (Team, 2013) to match each microprobe analysis from Saint Kitts with an experimental run from all experiments on the reference list in **Supplementary Table 1**. We searched for amphibole, clinopyroxene, orthopyroxene, olivine and plagioclase from experiments that matched ≥ (n-1) of the major elements in each phase to within 5% relative, where n is the number of major elements. K, Cr and Mn in mafic phases were omitted as they tend to be below detection or not consistently reported in experiments. These results can then be compared with P-T-X measured from our thermobarometers and chemometers, which is useful to estimate the performance of the trained algorithms.

Results

Mineral chemistry

Amphiboles form two visually discrete clusters (cluster 1 = SK408, SK385, felsic enclave from SK386B; cluster 2 = SK385, SK386B, SK388, SK390, SK394A, SK394C) in both Si vs Ca (**Fig. 3a**) and Mg vs Al (**Fig. 3b**). Both clusters show negative correlation for Si vs Ca, with cluster 1 ranging from 6.6 – 7.2 Si apfu (atoms per formula unit) compared with 6.0 – 6.5 apfu for cluster 2 (**Fig. 3a**). Given the strong negative correlation between amphibole Si and temperature (Putirka, 2016), this qualitatively suggests that cluster 1 formed at lower magmatic temperature than cluster 2. Cluster 1 shows negative correlation between Mg and Al, whereas cluster 2 shows positive correlation. Typically in the Eastern Caribbean these elements are positively correlated in amphibole for both experimental and natural samples (Martel et al., 2013; Melekhova et al., 2017; Pichavant et al., 2002) with a notable exception on Dominica (Solaro et al., 2019). For both Mg vs Al and Si vs Ca there is a significant compositional gap between the two clusters, suggestive of contrasting environments of formation. The SK385 amphiboles in cluster 1 are solely analyses from a reaction corona around orthopyroxene. Clinopyroxene exhibits a marked negative correlation between Mg and Al in SK392, compared to a moderate Al decrease with Mg in SK391 (**Fig. 3c**). Ca and Al positively correlate in clinopyroxene, with SK392 displaying higher Al for a given Ca compared to SK391 (**Fig. 3d**). In contrast to the felsic enclave in SK386B, the mafic enclave in SK392 spans identical mineral compositional space to its host rock. This implies that the enclave from SK392 was sampled from a similar source region as its host whereas the SK386B enclave is antecrystic *sensu lato.*

Thermobarometry uncertainty estimates

An example of one of the 200 models (where each model employs a different test and train dataset split) for the TB(A) and TB(C) can be seen in **Fig. 4**. Amphibole is a remarkably sensitive thermobarometer, producing faithful predictions with low residuals across the full range of temperature (**Fig. 4a**) and pressure (**Fig. 4b**). Clinopyroxene is reliable from 900 – 1250 ˚C, although underestimates at lower temperature (< 900 ˚C; **Fig. 4c**). Clinopyroxene produces decidedly more scatter in pressure than amphibole (**Fig. 4d**). Each resampling of the test and train dataset generates a slightly different model based on the difference in data in the resampled train dataset. This produces a distribution of SEEs for all 200 models (**Fig. 5**). We take the modal uncertainty for each of these distributions as the uncertainty to be associated with a given estimate of natural data: pressure uncertainties of 1.4 kbar and 2.3 kbar for amphibole and clinopyroxene respectively (**Fig. 5a**), and temperature uncertainties of 40 ˚C and 65 ˚C for amphibole and clinopyroxene respectively (**Fig. 5b**). Using cations or oxides makes negligible difference to the performance of the thermobarometers (**Fig. 5**). We argue against using site-specific mineral chemistry (e.g., tetrahedral, octahedral) as these rely on assumptions for filling of cation sites, particularly in amphibole, which may bias results.

Amphibole as a reliable thermobarometer

Amphiboles are host to a wide array of cation substitutions (Leake et al., 1997), attributed to changes in intensive parameters (Blundy and Cashman, 2008). However, amphibole chemistry is more sensitive to temperature and melt composition than pressure variability. This has historically resulted in good performance of amphibole thermometers (Holland and Blundy, 1994; Putirka, 2016) and chemometers (Zhang et al., 2017), alongside equally poor performance of amphibole barometers (Ridolfi and Renzulli, 2012), with the exception of those applied in multiply-saturated granitic systems (Anderson and Smith, 1995). The excellent performance of our amphibole barometer (**Fig. 4; Fig. 5**) is at odds with these previous studies. Indeed, amphibole performs significantly better as a barometer than clinopyroxene.

To rationalise this discrepancy, and assess its robustness, we compare the TB(A) to an amphibole thermobarometer developed using linear regression (Ridolfi et al., 2010; Ridolfi and Renzulli, 2012). We use the test dataset of Erdmann et al (2014), who questioned the ability of amphibole to recover magmatic pressures, which spans lower – mid crustal pressures (2 – 4 kbar) and a range of magmatic temperature (800 – 1000 ˚C). Results from the TB(A) show a pressure SEE of 0.71 kbar for the test dataset of Erdmann et al (2014), with 93% of pressures recovered to within 1 kbar of the experimental pressure (**Fig. 6a**). This represents a remarkable improvement compared with the approach of Ridolfi and Renzulli (2012). As is expected from the results of Ridolfi and Renzulli (2012) and Erdmann et al (2014), temperature estimates (**Fig. 6b**) from amphibole are good (SEE = 23 ˚C), with the TB(A) showing substantially less scatter than that of Ridolfi and Renzulli (2012).

Multiple-reaction barometers may offer a robust estimate of pressure, with the limitation of requiring a suite of equilibrated, touching phases. The spinel-clinopyroxene-olivine-plagioclase (SCOlP) barometer of Ziberna et al (2017) provides an equilibration pressure of olivine-bearing enclaves from Dominica (Ziberna et al., 2017) and Saint Kitts (Melekhova et al., 2017) with uncertainties of 0.9 – 2.6 kbar. To further test our barometer, we take Saint Kitts samples from Ziberna et al (2017) that coexist with amphibole and compare the results for amphibole rims to the predicted pressure derived from SCOlP. This offers a metric to evaluate the uncertainty of the TB(A) on natural samples with well-constrained intensive parameters. **Fig. 6c – d** shows the offset between pressure and temperature predicted using the TB(A), and the estimates of Ziberna et al (2017). All inclusions have a temperature, according to Ziberna et al (2017), of 950 ˚C ±50 (**Fig. 6c**). All TB(A) estimates are within the error of ±50 ˚C from Ziberna et al (2017), showing excellent agreement for temperature between the two systems. The exception is a single point from sample KS31 (a plutonic inclusion; interpreted as a fragment of magmatic mush; Melekhova et al., 2017) which has a lower predicted temperature than that of Ziberna et al (2017). This point is a chemical outlier relative to the other samples, with low Mg, high Fe, and very high Mn, explaining the offset in temperature. Pressure estimates (**Fig. 6d**) also show strong agreement between the two barometers, particularly for the inclusions at 2 kbar which are estimated by the TB(A) as precisely 2 kbar. Estimates of the two samples

(KS7 and KS8 from Melekhova et al., 2017) at 6 kbar by Ziberna et al (2017) span 4 – 6 kbar according to the TB(A). This demonstrates that the TB(A) can effectively discriminate between upper and middle crustal pressures in Saint Kitts amphiboles.

The inferred pressure sensitivity of amphibole suggests that the machine learning algorithm can recover more nuanced, non-linear relationships between phase chemistry, pressure, and temperature than traditional regression approaches. Hence, we argue that it is the regression strategy, as opposed to the insensitivity to pressure, that hinders previous calibrations of amphibole barometers. This is demonstrated by the agreement between the TB(A), equilibrium experiments (**Fig. 4**; **Fig. 6a – b**), and independent multiple-reaction barometers (SCOlP; **Fig. 6c – d**) for a range of compositions and conditions. This conclusion allows us to interrogate the variation of pressure and temperature in the Lower Mansion Series, recorded by amphibole, with confidence.

P-T-X estimates for the Lower Mansion Series

The range of estimated crystallisation pressure for each of the Lower Mansion Series samples are shown in **Figure 7a**. SK408 (basal pyroclastic flow) has a restricted pressure of 1.8 – 2.1 kbar. The base of the Mansion Series (SK385) yields higher pressure with respect to SK408, spanning from 2 – 4.5 kbar and a mean of 3.8 kbar. Along the stratigraphy from SK385, pressure consistently decreases to a mean of ~ 2 kbar for SK391, before widening significantly in pressure extent for SK392 (**Fig. 7a**). The uppermost units (SK394A; SK394C) span 2.7 – 5 kbar. Overall, this suggests the majority of differentiation associated with the Mansion Series magmatism is consistently occurring at ~ 2 – 4 kbar (the middle – upper crust) for samples that contain amphibole. Temperature systematically increases from the basal pyroclastic flow (820 ˚C) to SK391 (1010 ˚C), with a slight drop in temperature in SK394A and SK394C (**Fig. 7b**). Ranges of temperature for each sample are relatively tight (< 60 ˚C) with the exception of SK391 which shows a wider temperature range. Temperature positively correlates with modal An# in the matrix plagioclase, suggesting that this An# increase is being thermally controlled (**Fig. 7c**). However, plagioclase inclusions in amphibole are consistently An# 80 – 90, with the exception of SK408, raising questions about whether such inclusions are in equilibrium with their host phase (see Discussion).

The chemistry of melts predicted by amphibole and clinopyroxene chemometers (Al_2O_3, K_2O, CaO, Na_2O, MgO, FeO) plotted versus SiO_2 as a measure of differentiation are shown in **Figure 8**. Predicted SiO_2 and Al_2O_3 of amphibole melts negatively correlate (**Fig. 8a**). Clinopyroxene melts show a shallower decrease of SiO_2 versus Al_2O_3, initiating from ~ 17.5 wt% Al_2O_3 at ~ 52 wt% SiO_2 (**Fig. 8a**). Only predicted melts from SK394C consistently overlap with the high-Al basalt (> 19 wt% Al_2O_3) whole rock samples erupted on Saint Kitts (**Fig.**

8a). Melt K_2O from amphibole increases with increasing SiO_2 from ~ 0.5 – 2.5 wt%, accordant with a low-K system in which K is incompatible (**Fig. 8b**). The CaO, Na_2O, MgO, and FeO of predicted melts (**Fig. 8c, d, e, f**) plot concordantly with whole rock trends on Saint Kitts, although recalculated melts tend to have lower FeO (**Fig. 8f**) and slightly lower CaO (**Fig. 8c**) than a whole rock of equivalent SiO_2. Melts predicted from amphibole in SK408 match closely with glass measurements from the same sample for all elements, implying that amphibole is in equilibrium with the matrix glass (**Fig. 8f**). In general, some samples (SK408, SK385) display a tight range of melt composition whereas others (SK390, SK391, SK392, SK394C) cover a much wider range, correspondent with their span of mineral chemistry (**Fig. 3**).

Comparison with equilibrium experiments

Figure 9 shows a comparison between natural, experimental and thermobarometric information derived from silicate phases. Matches of experimental An# with natural plagioclase phenocrysts, matrix, or inclusions, do little to constrain pressure or temperature. Whilst An# of plagioclase increases strongly with temperature, the overprinting effect of water content and starting composition produces wide fields (**Fig. 9**). Matching experimental amphibole (**Fig. 9a – e**; **Fig. 9h**; **Fig. 9i**) and clinopyroxene (**Fig. 9f**; **Fig. 9g**) with EPMA analyses produces much more constrained pressure-temperature fields in many cases, particularly for temperature (e.g., SK408, SK388, SK394A, SK394C). This is logically the case for amphibole as by matching only Si, the temperature is relatively well constrained (Putirka, 2016). In almost all cases matched clinopyroxene and amphibole from experiments overlap with thermobarometric fields, providing a useful validation of the thermobarometry method. Plagioclase in equilibrium with clinopyroxene and amphibole experimental matches (filled circles in **Fig. 9**) that overlap with thermobarometry PT estimates (filled polygons **Fig. 9**) can be used as a metric to infer the An# of the co-crystalising plagioclase. Plagioclase inclusions in amphibole are An# 80 – 90 with the exception of SK408 (**Fig. 7**). However, experimental plagioclase in apparent equilibrium with natural amphibole and clinopyroxene consistently falls outside of inclusion chemistry. Matrix plagioclase from natural samples matches much more closely with experimental co-crystallising plagioclase, accordant with the correlation between thermometer temperature and matrix An# (**Fig. 7c**). This suggests inclusions are poor records of equilibrium plagioclase composition, in particular for Saint Kitts amphiboles.

Discussion

P-T-X-H_2O versus time in the Lower Mansion Series

The crustal column beneath a volcanic edifice is a thermally and chemically stratified sequence of magmatic minerals (Sparks et al., 2019). This is reflected in the array of phenocryst chemistry and textures from lavas, pyroclastics, and enclaves erupted at a single centre (e.g. Klaver et al., 2018, 2017). Magma may remain resident in the system for long periods, move through relatively unimpeded, or never reach the surface. An evolved crustal column may act as an efficient density (and, by extension, composition) filter for magma (Stolper and Walker, 1980). Understanding these processes necessitates the recovery of the key magmatic variables that control the eruptive dynamics of a volcano: pressure (**Fig. 7a**); temperature (**Fig. 7b**); melt composition (**Fig. 8**); melt water content. The latter requires direct H_2O measurement of mineral-hosted melt inclusions (Danyushevsky et al., 1993; Hervig et al., 1989; Zajacz et al., 2005), hygrometry (Waters and Lange, 2015), or calculation of melt H_2O using partition coefficients derived from nominally anhydrous minerals (e.g. clinopyroxene and orthopyroxene; Edmonds et al., 2016; Hauri et al., 2006). Melt inclusions may be entirely absent in crystals or disproportionately represented in certain domains (core or rim) due to a propensity to form along cracked surfaces (Faure and Schiano, 2005) or during discrete heating, dissolution, and reprecipitation events (Cashman and Blundy, 2013; Edmonds et al., 2016; Nakamura and Shimakita, 1998). Indeed, amphibole-hosted melt inclusions in Saint Kitts samples are sparse. To overcome this, we combine melts from amphibole chemometry (this study) with the modal plagioclase matrix composition (**Fig. 7c**; Higgins et al., 2021) to give a series of plagioclase – melt pairs. These plagioclase – melt pairs were used in the hygrometer of Waters and Lange (2015) which can predict melt water content with an SEE of 0.35 wt%. We assess whether these melts are saturated in a vapour phase using equation 10 in Zhang et al (2007) at the conditions described by our thermobarometers. For clinopyroxene bearing samples, hygrometer calibrations for specific melt compositions exist (e.g. alkaline Etnean magmas; Armienti et al., 2013; Perinelli et al., 2016), although globally applicable calibrations are lacking. Instead, we use estimates from experimental matches (**Fig. 9**) to infer melt water contents in equilibrium with Saint Kitts clinopyroxene where possible.

The samples from the Lower Mansion Series show a progressive temperature increase, evidenced through matrix plagioclase An# increase and thermometry (**Fig. 7b; Fig. 7c**), coupled with relatively stable barometric estimates for several deposits (**Fig. 7a**). We will now place this into the context of the evolving sub-volcanic system, using our full P-T-X-H_2O versus (relative) time dataset (**Fig. 10**).

Clearing out the pipes of the magma plumbing system

The lower pressure of SK408 (~2 kbar) compared to the majority of the sequence (**Fig. 7a**), along with its experimental phase assemblage matches (**Fig. 9**), indicates protracted residence in the upper crust: rhyolitic glass, orthopyroxene, amphibole, plagioclase and Fe-oxides are found in a subset of similar pumice from Dominica that have been linked to upper crustal differentiation (Solaro et al., 2019). Quartz grains in SK408 can be ascribed to prolonged cooling in the upper crust in equilibrium with rhyolitic glass and albitic plagioclase (Solaro et al., 2019). Late stage resorption (rounding) is invoked by the contraction of the cotectic in the An-Ab-Qtz ternary (granite minimum) towards the quartz end member during decompression (Ghiorso and Gualda, 2015). The match between the predicted liquid from amphibole chemometry (**Fig. 8**) and the rhyolitic glass from SK408 implies amphibole was a late crystallising phase. Hence the TB(A) records a robust estimate of final equilibration conditions in SK408. Therefore, we suggest that SK408 acted as an upper-crustal plug to the volcanic plumbing system. As such, the pronounced compositional gap for magmas (pyroclastics or lavas) at 66 – 72 wt% SiO_2 on Saint Kitts could reflect an intrinsic feature of melt production: melt that evolves beyond ~66 wt% SiO_2 is difficult to erupt in large quantities. Therefore, eruptions of magmas with > 66 wt% SiO_2 are restricted to rare dome effusions (e.g., the Salt Pond Dome; Baker, 1984), as rhyolitic glass in upper crustal bodies following protracted cooling (SK408), or slithers of evolved, interstitial melt erupted inside fragments of the deeper plutonic system (Melekhova et al., 2017; this study). Mineral-hosted (predominantly clinopyroxene and plagioclase; **Fig. 8a**) melt inclusions fill this compositional gap and are typically erupted in magmas with < 66 wt% SiO_2 (**Supplementary Fig. 3**; Cooper et al., 2020; Melekhova et al., 2017). An analogue to this in the Eastern Caribbean may be Bequia (Camejo-Harry et al., 2018) where melts are consistently more evolved than concomitant lavas, revealing a lack of either sufficient size or efficient melt extraction in the magmatic system. A rare exposed window into an equivalent plutonic regime may be found on Saint Martin in the north of the extinct Limestone Caribbees where the evolved granodiorite pluton spans 62 – 75 wt% SiO_2 (Davidson et al., 1993). Given the assertion that amphibole crystallised in equilibrium with the matrix glass we can also be confident that the predicted melt water content (6.1 wt% H_2O; water saturated at 2 kbar; **Fig. 10**) is indicative of the final, pre-eruptive melt water content for SK408.

Progressive increase of temperature in time

Removing this chemically evolved, upper-crustal plug permitted less evolved material to be erupted from the middle – upper crust (2 – 5.5 kbar; **Fig 7a**; **Fig. 10**). Magmatic temperatures increase consistently along with An# of matrix plagioclase. Although constraining a timescale from palaeosoils is difficult due to highly variable accretion rates in the Caribbean, the sparse palaeosoils between SK386B and SK390 imply this increase is happening over short (decadal to millennial) timescales (Higgins et al., 2021). As thicker deposits (e.g., SK390 and SK391) tend to sample a wider variety of plagioclase phenocryst chemistry (Higgins et al., 2021), the mechanism that generates larger volume eruptions is not necessarily coupled to the thermal maturation at this temporal scale. Relationships between erupted volume and deposit thickness are likely to hold true at the proximity to the source of the Mansion Series stratigraphy in this study (**Fig. 1**), as shown by mapping of dispersal characteristics on Saint Kitts (Roobol et al., 1985).

Melt water content from hygrometry reveals a relatively limited range from 5 – 6.7 wt% H_2O. This is in excellent agreement with water contents of Saint Kitts melt inclusions (Cooper et al., 2020; Melekhova et al., 2017). All amphibole melts from SK385, SK386B, SK388, and SK390 are water-undersaturated according to equation 10 of Zhang et al (2007). The felsic enclave in SK386B is an exception, with melts recording the same water-saturated conditions as SK408. In fact, the similar mineralogy, water content (**Fig. 10**), pressure (**Fig. 7a**), temperature (**Fig. 7b**), and melt chemistry (**Fig. 8**) between the felsic enclave in SK386B and sample SK408 suggests the former could be the plutonic (intrusive) equivalent of the latter, scavenged during ascent through the upper crust.

Peak thermal maturity reflected in clinopyroxene – amphibole phase relations

In SK391 and SK392, clinopyroxene is present as phenocrysts and amphibole is absent. This agrees with the examination of our experimental database which shows that, at middle to upper crustal conditions, the Saint Kitts magmas lie outside of any stability field in which amphibole and clinopyroxene coexist. Instead, olivine and clinopyroxene crystallise at the expense of amphibole. This is a well-established incongruent thermal reaction driven by decreasing temperature (liquid + clinopyroxene $\rightarrow$ amphibole), observed in experimental (Foden and Green, 1992) and natural (Smith, 2014) samples including Lesser Antilles enclaves (Cooper et al., 2016; Melekhova et al., 2017). Therefore the crystallisation of clinopyroxene and amphibole from high-Al basalts (Andújar et al., 2015; Foden and Green, 1992; Melekhova et al., 2017; Melekhova et al., 2021) and dacites (Marxer and Ulmer, 2019; Pichavant et al., 2002; Solaro et al., 2019) equivalent to inferred Saint Kitts starting compositions can impart information about the thermal balance establishing in the system through time (**Fig. 10**). Effectively, the amphibole – clinopyroxene transition is merely reflecting the thermal state of the magma beneath Saint Kitts (phase boundaries in **Fig. 10**). Peak temperatures are represented by SK391 and SK392 which have crossed into the clinopyroxene field. Higher temperature amphibole melts (SK386B, SK390) lie closer to the "amphibole in" boundary, with decreasing temperature driving amphibole melts to higher SiO_2 (**Fig. 9b**). More evolved (cooler) melts that lie further from this boundary should crystallise less anorthitic plagioclase (e.g., SK385), in agreement with matrix plagioclase mineral chemistry (Higgins et al., 2021).

The difference between clinopyroxene and amphibole thermobarometry estimates on Saint Kitts is mirrored in their equilibrium melt chemistry (**Fig. 8**). Al_2O_3 shows a decrease versus SiO_2 for clinopyroxene melts (**Fig. 8a**). This is typical of melts saturated in plagioclase (Grove et al., 2012; Sisson and Grove, 1993). Considering decreasing Mg as an indicator of progressive differentiation, and that calcic plagioclase is one of the dominant sinks of Al in arc magmas, we would expect Al in clinopyroxene to decrease with decreasing Mg in the presence of abundant plagioclase (Klaver et al., 2017). In SK392 the opposite is true (**Fig. 3c**), despite predicted melt chemistry that attests to plagioclase saturation. Combined, these melt and mineral chemistry features represent two competing effects. Firstly, plagioclase saturation increases Al-activity in the melt, increasing Al with decreasing Mg in clinopyroxene, as noted in experimental studies (Nandedkar et al., 2014; Villiger et al., 2007). Secondly, the clinopyroxene to plagioclase ratio is affected by melt water content. At fixed pressure and temperature, and increasing water activity, the ratio of clinopyroxene to plagioclase increases. This is because water destabilises plagioclase but has less effect on clinopyroxene abundance at these conditions (Andújar et al., 2015; Sisson and Grove, 1993). Therefore, we suggest that the clinopyroxene from SK392 represents crystallisation from a wet, but water-undersaturated, high-Al basalt that cooled between 1025 ˚C and 950 ˚C. This cooling would largely explain the range of melt chemistry from the clinopyroxene chemometer (**Fig. 8**) as well as the increase in Al in the clinopyroxene during differentiation, resulting from an increase in melt H_2O (suppressing plagioclase) during crystallisation. The subtle balance between clinopyroxene and plagioclase mineral fraction is mirrored in the shallower trend in melt Al_2O_3 versus SiO_2 (**Fig. 8a**), indicative of a smaller fraction of plagioclase than coexists with the amphibole melts. Amphibole melts show the same decrease in Al_2O_3, albeit with a trend that initiates from a higher initial Al_2O_3 than the clinopyroxene melts (**Fig. 8a**). Amphibole from SK394C records a notably higher Al_2O_3 content than any other sample. This suggests a more protracted stage of fractionation of Al-poor phases (olivine, clinopyroxene, orthopyroxene, spinel) prior to plagioclase saturation. The slightly hooked appearance of the Al_2O_3 versus SiO_2 trend may even indicate the final moments of a melt at the cusp of plagioclase saturation. The larger degree of fractionation of the parent melt to the amphiboles of SK394C is also reflected in its melt water content, the highest of any sample (modal peak of 6.5 wt% H_2O; **Fig. 10b**).

Cryptic fractionation from andesitic melts unveiled by amphibole chemometry

A feature of melt inclusion records in arc magmas is a pronounced bimodality in SiO_2 (wt%), whereby melt inclusion chemistry correlates poorly with host bulk rock chemistry in the andesitic range (Reubi and Blundy, 2009). However, results from amphibole chemometry show a large proportion of melts with 55 – 65 wt% SiO_2, covering much of the spectrum that is conspicuously absent in melt inclusions (**Fig. 8a**). This suggests that amphibole chemometry effectively reveals cryptic andesitic melts within the volcanic sub-system. Cryptic evolved melts are recorded in plagioclase via a similar process in the monotonous basaltic magmas of the Gálapagos (Stock et al., 2020). Upon amphibole crystallisation, the surrounding melts are chemically propelled from andesitic composition towards more silicic melts via two effects. Firstly, amphibole exerts a large differentiation effect on the melt due to its low silica content relative to other common fractionating silicates in arc systems. Secondly, amphibole generally appears in the "liquid line of descent" at a point where arc magmas spend a relatively short period of time, resulting in rapid differentiation and a low occurrence probability of andesitic melts (Caricchi and Blundy, 2015; Marsh, 1981; Müntener and Ulmer, 2018; Nandedkar et al., 2014). Based on this evidence amphibole may have a significant effect not just on trace element behaviour (Davidson et al., 2007; Smith, 2014) but also on major element behaviour in arc magmas.

Late-stage waning

In the overall trend of the sequence, SK394A and SK394C represent a minor, late-stage thermal waning that results in re-crossing of the amphibole – clinopyroxene cotectic (**Fig. 10b**). However, these samples also appear to be more representative of the dominant magma composition in the sub-volcanic system. This is revealed by textural segmentation of quantified chemical maps (Higgins et al., 2021; Sheldrake and Higgins, 2021) which show an increased abundance of homogeneous, high-An# crystals in the upper units of the stratigraphy, as well as mean An# of matrix plagioclase and phenocryst plagioclase converging to near uniformity. The appearance of a less-evolved composition is preserved almost entirely in the mineral chemistry, with the bulk rock from the Lower Mansion Series broadly overlapping with the most common composition erupted throughout the history of Saint Kitts volcanism (an andesite with ~58 wt% SiO_2 and ~17.4 wt% Al_2O_3; **Supplementary Fig. 3**). This contrasts with the varied mineral chemistry and textures, particularly in plagioclase (Higgins et al., 2021; **Fig. 7c**; **Fig. 9**).

The observable disequilibrium between plagioclase inclusions in amphibole and amphibole temperature may be explained by a similar process. Essentially the melt and the crystal column through which it moves are chemically decoupled from one another. Ascending melts that crystallise amphibole may cannibalise small, high-An# crystals that reveal the dominant chemistry in the subvolcanic region but not necessarily the crystal in equilibrium with the package of melt from which the amphibole crystallised. As the magmas leaving the top of the system transition to a more representative composition of the magmatic system in time (e.g., SK394A, SK394C), the plagioclase inclusion chemistry, phenocryst chemistry and matrix chemistry converge. Such an observation is unsurprising considering an identical process occurs in plagioclase phenocrysts in the form of rare, high-An# cores in SK408 (Higgins et al., 2021). This process is consistent with "petrological cannibalism" whereby chemically and spatially disparate crystals from the plutonic sub-system are scavenged and amalgamated into a final erupted product (Cashman and Blundy, 2013; Davidson et al., 2007; Reubi and Blundy, 2008). An# of inclusions would not re-equilibrate with the host amphibole due to the slow rates of CaAl–NaSi interdiffusion in plagioclase at magmatic temperatures (Grove et al., 1984), which may even surpass cooling timescales of some magma reservoirs (Pichavant et al., 2007). Resorption could not occur as the plagioclase is entombed in its host and is therefore chemically isolated from the reactive magma volume (Pichavant et al., 2007). Our observations raise questions surrounding the validity of using inclusions in amphibole as equilibrium pairs for thermobarometry.

Evidence for a vertically extensive magmatic system?

Evidence from modelling, geochemistry, and geophysics over the last two decades asserts that magmatic systems should be considered as transcrustal entities (Annen et al., 2006; Christopher et al., 2015; Sparks et al., 2019). One of the key features of these systems is that much of the differentiation is staged in the deep crust, which acts as a factory for cumulate textured rocks, whereas the middle – upper crust is a vertically extensive system that hosts more ephemeral bodies of melt and crystals (Annen et al., 2006; Cashman et al., 2017; Hildreth and Moorbath, 1988; Jackson et al., 2018). The results of our thermobarometry add support to this view. The depth range of the inferred magmatic system beneath Saint Kitts extends from 2 kbar to ~5.5 kbar, equivalent to a depth of 3 – 15 km (crustal density 2.7 g/cm^3; **Fig. 10**). This is consistent with the vertical extents for the upper portion of inferred transcrustal magmatic systems beneath stratovolcanoes in the Eastern Caribbean (Camejo-Harry et al., 2018; Christopher et al., 2015; Cooper et al., 2016; Edmonds et al., 2014) and elsewhere (Cashman and Blundy, 2013). In general, there is a moderate increase in the vertical extent (pressure range) over which crystallisation occurred, coincident with clinopyroxene crystallisation (**Fig. 10**). Critically, however, the majority of magma released by the investigated eruptions (except SK408) are sourced from a significant range of depth in the crust (**Fig. 7**; **Fig. 10**).

The sub-vertical pressure-temperature gradient on Saint Kitts (**Fig. 10**), present throughout the eruption history, suggests that magmas were erupting from a thermally mature crust: if the crust was to have a pristine geothermal gradient, shallower magmas should be much cooler than deeper magmas (Karakas et al., 2017) which is not the case on Saint Kitts. However, the uncorking of the upper crustal system (SK408) likely removed a significant amount of heat from the system. Therefore, if we consider a rather constant average long-term magma flux (e.g. Caricchi, 2013), the eruptive sequence on Saint Kitts reflects a thermal contraction as the system recovers to its steady state. Recovery may be signified by the point at which the matrix plagioclase, phenocryst plagioclase, and inclusion chemistry in amphibole converge (i.e., the upper units of the series; **Fig. 7**; **Fig. 10**; Higgins et al., 2021). The composition at which they converge is An# 80 – 90, the most abundant phenocryst chemistry throughout the Lower Mansion Series sequence (Higgins et al., 2021), and therefore the most sampled inclusion chemistry. The dominance of relatively unzoned, anorthite-rich plagioclase in cumulate textured enclaves on Saint Kitts supports this view (Melekhova et al., 2017).

Conclusions

We have calibrated a clinopyroxene-only and amphibole-only thermobarometer that yield performance comparable to (in the case of clinopyroxene; **Fig 4c**; **Fig. 4d**) and far exceeding (in the case of amphibole; **Fig 4a**; **Fig. 4b**) that of existing thermobarometers (Petrelli et al., 2020; Ridolfi et al., 2010; Ridolfi and Renzulli, 2012). Equilibrium experiments, as well as natural samples with well-constrained pressure and temperature, were used to independently verify the performance of the amphibole thermobarometer, in many cases recovering pressures to within ~ 1kbar of known values (**Fig. 8**). This suggests that amphibole acts as a reliable indicator of magma storage pressure and temperature without requiring multiple saturation conditions with liquid or other solid phases. Machine learning regression uncovers subtle relationships between intensive parameters and mineral chemistry, unaccounted for by conventional linear regression approaches (e.g. Ridolfi and Renzulli, 2012). Chemometers, recorders of melt chemistry in equilibrium with a mineral phase, delineate evolution trends in excellent agreement with those elucidated by whole rock and melt inclusion chemistry from Saint Kitts (**Fig. 7**). The ability to predict melt chemistry has wide-reaching future applications in Earth sciences, including combination with viscosity models (Giordano et al., 2008).

Thermobarometry and chemometry (this study), coupled with hygrometry (Waters and Lange, 2015), have allowed us to unpick the P-T-X-H_2O versus time of the evolving sub-volcanic reservoir beneath Saint Kitts (**Fig. 6**; **Fig. 9**). The basal pyroclastic flow removed an upper-crustal plug that had formed at ~2 kbar, allowing progressively hotter, amphibole-saturated magma to move through from depth (2 – 5.5 kbar). Continuous increase in temperature resulted in the crossing of a cotectic, forming clinopyroxene at the expense of amphibole (Foden and Green, 1992). Frozen snapshots of this incomplete reaction can be found in the plutonic magmatic inclusions erupted on the island (Melekhova et al., 2017). Thermobarometry and chemometry of amphibole and clinopyroxene were paired with equilibrium experiments that match closely to their mineral chemistry. This identified disequilibrium in amphibole-hosted plagioclase inclusions. The magma most representative of the subvolcanic reservoir beneath Saint Kitts is reflected in the uppermost units (SK392 – SK394C) where plagioclase phenocrysts, matrix and inclusions become relatively chemically invariant.

Compared with multi-reaction barometers that rely on melt or equilibrium pairs, the TB(A) and TB(C) can record the entire history of each crystal. This drastically increases the probability of sampling the true extent of the magmatic system. Bias may be introduced when melt or matrix chemistry is used in liquid-dependent thermobarometers: pressure estimates are skewed towards lower pressures as matrix melt was crystallised last and is more likely to have equilibrated in the shallowest portion of the magmatic system. Hence the global estimate of 2 kbar for most upper-crustal magmatic systems (e.g. Plank et al., 2013) is likely an absolute minimum, representing the roof as opposed to the main thermal engine of a volcanic plumbing system.

Our approach has facilitated a link between an eruptive cycle for an arc volcano (Mount Liamuiga, Saint Kitts) and the intensive parameters that govern eruptive behaviour. This is particularly important in a system where whole-rock variation clearly masks much of the nuances uncovered using mineral chemistry (this study; Higgins et al., 2021) which may not be the case in certain unique examples (Gertisser and Keller, 2003). By extending our approach to other volcanic systems we may better uncover the links between the temporally evolving chemical and physical properties of magma and the eruptive behaviour of volcanoes.

Figure Captions

Fig. 1. (**a**) Geological map of Saint Kitts, Lesser Antilles, modified after Martin-Kaye (1959). The four volcanic centres young towards the north west. The active centre is Mt Liamuiga which is responsible for the deposition of the Mansion Series. Peléan Style volcanic domes of various ages outcrop across the island (e.g., Baker, 1968). Study locality is a sea cliff showing a well-exposed pyroclastic fall sequence between the villages of Mansion and Tabernacle. **(b)** Stratigraphic sequence that is the focus of this study. A basal pyroclastic flow deposit (sample SK408) separates the Lower Mansion Series (Unit A – C according to Roobol et al., 1981)

Fig. 2: Amphibole and clinopyroxene bearing experiments used to train the models for the thermobarometers presented in this study. Note that amphibole stability is thermally dependent (≤ 1050˚C). Clinopyroxene spans a wider range of temperatures at a given pressure. Both phases are stable across the pressure range studied (0.002 – 12 kbar), although amphibole stability requires lower temperature at lower pressure (dashed line). Arrows with chemical element labels indicate qualitative relationships between pressure, temperature, and phase composition [1200, 831]

Fig. 3: Cation variation diagrams for amphibole (23 oxygens) and clinopyroxene (6 oxygens). Panels are Si vs Ca (**a**) and Mg vs Al (**b**) for amphibole and Ca vs Al (**c**) and Na vs Mg (**d**) for clinopyroxene

Fig. 4: Binary plot reporting the pressure and temperature prediction of a test dataset for amphibole (a; b) and clinopyroxene (c; d). Models represent estimations for one of the 200 repetitions of the splitting of the test and train datasets. In this case the model selected is the best performing (lowest SEE) of the 200 repetitions [1200,1028]

Fig. 5: Standard error estimate (SEE) distributions for test datasets for each of the 200 splits of test and train datasets. (a) Pressure SEE distributions for amphibole and clinopyroxene. (b) Temperature SEE distributions for amphibole and clinopyroxene. Note that for both pressure and temperature, models using cations show very little difference compared to models using oxides [1200, 702]

Fig. 6: Performance of amphibole barometer assessed using: (a) experimental pressure; (b) experimental temperature; (c) natural temperature; and (d) natural pressure as comparators. Experimental samples from the dataset of Erdmann et al (2014) are compared to predictions by the amphibole only thermobarometer of Ridolfi et al (2010; RR10) and Ridolfi and Renzulli (2012; RR12). Natural samples are amphibole rims from Saint Kitts magmatic inclusions (Melekhova et al., 2017) which appear in Ziberna et al (2017). Black error bars are reported from Ziberna et al (2017)

Fig. 7: Distribution of pressure (**a**), temperature (**b**), and plagioclase chemistry (**c**) for Saint Kitts amphibole (black outlined barplots) and clinopyroxene (grey outlined barplots). Light brown bars indicate palaeosoils, grey bars indicate units analysed in this study, white bars indicate other volcanic units (Higgins et al., 2021) [1288, 695]

Fig. 8: Binary geochemical Harker plots for all elements predicted by amphibole and clinopyroxene chemometry in the Lower Mansion Series. Uncertainties for chemometers are quoted in Supplementary Table 1. Data sources: this study; Baker, 1984, 1968; Higgins et al., 2021; Melekhova et al., 2017; Toothill et al., 2007 [1291, 749]

Fig.9: Comparator plot for natural, experimental, and thermobarometry data relevant to each unit from the Lower Mansion Series. An extensive experimental dataset (references from Supplementary Table 1) has been subsetted so as to match Saint Kitts mineral compositions (see text for details). This enables the recovery of pressure and temperature fields. In general, amphibole and clinopyroxene fields are much more constrained than plagioclase, orthopyroxene or olivine

Fig.10: Snapshots (a, b) of the magmatic system of Saint Kitts as recorded by the eruptive products of the Lower Mansion Series, using amphibole and clinopyroxene thermobarometry. Basalt clinopyroxene – amphibole phase boundaries: Foden and Green (1992). Dacite clinopyroxene – amphibole phase boundaries: Marxer and Ulmer (2019); Solaro et al (2019) [892,693]

Supplementary Fig. 1: Pairs plots of data used to calibrate amphibole only (a) and clinopyroxene only (b) thermobarometers. Data are cations on the basis of 23 and 6 oxygens respectively (all Fe as FeO) [850, 781]

Supplementary Fig. 2: A single decision tree cut at level 4 for determination of temperature (˚C; end of branches) on the basis of cation chemistry. Note that a subset of the predictor variables (Ti, Al, Fe, Na, Mn) are used in a single tree as opposed to all predictor variables. This is termed “feature randomness” and is designed to create trees that are as uncorrelated with one another as possible. Once the structure of each tree has been created during the machine learning process, analyses with unknown temperature (e.g., Saint Kitts analyses) are cascaded through all of the decision trees in the forest to arrive at a temperature by means of the temperature with the most votes (i.e., a wisdom of the crowd approach)

Supplementary Fig. 3: SiO_2 (wt%) and Al_2O_3 (wt%) histograms for Saint Kitts volcanics. Dashed lines show modal values. Data sources: this study; Baker, 1984, 1968; Higgins et al., 2021; Melekhova et al., 2017; Toothill et al., 2007 [1291, 749]

Supplementary Table 1: Table of experiments used to calibrate the amphibole only (a) and clinopyroxene only (b) thermobarometers

Supplementary Table 2: Mode and range (minimum and maximum) standard error estimates (SEE) for temperature-dependent amphibole and clinopyroxene chemometers (SiO_2, Al_2O_3, CaO, Na_2O, K_2O, MgO, FeO) in wt%. SEE modes and ranges are derived from n = 200 models with variable splitting of test and train datasets, mirroring the method used for thermobarometers. See text for details

References

Al'meev, R.R., Ariskin, A.A., Ozerov, A.Y., Kononkova, N.N., 2002. Problems of the Stoichiometry and Thermobarometry of Magmatic Amphiboles: An Example of Hornblende from the Andesites of Bezymyannyi Volcano, Eastern Kamchatka 40, 16.

Anderson, J.L., Smith, D.R., 1995. The effects of temperature and f_{O2} on the Al-in-hornblende barometer. American Mineralogist 80, 549–559. https://doi.org/10.2138/am-1995-5-614

Andújar, J., Scaillet, B., Pichavant, M., Druitt, T.H., 2015. Differentiation conditions of a basaltic magma from Santorini, and its bearing on the production of andesite in arc settings. Journal of Petrology 56, 765–794.

Annen, C., Blundy, J.D., Sparks, R.S.J., 2006. The Genesis of Intermediate and Silicic Magmas in Deep Crustal Hot Zones. J Petrology 47, 505–539. https://doi.org/10.1093/petrology/egi084

Arculus, R.J., Wills, K.J., 1980. The petrology of plutonic blocks and inclusions from the Lesser Antilles island arc. Journal of Petrology 21, 743–799.

Armienti, P., Perinelli, C., Putirka, K.D., 2013. A New Model to Estimate Deep-level Magma Ascent Rates, with Applications to Mt. Etna (Sicily, Italy). Journal of Petrology 54, 795–813. https://doi.org/10.1093/petrology/egs085

Baker, P.E., 1985. Volcanic hazards on St Kitts and Montserrat, West Indies. Journal of the Geological Society 142, 279–295. https://doi.org/10.1144/gsjgs.142.2.0279

Baker, P.E., 1984. Geochemical evolution of St Kitts and Montserrat, Lesser Antilles. Journal of the Geological Society 141, 401–411. https://doi.org/10.1144/gsjgs.141.3.0401

Baker, P.E., 1980. Geology and geochemistry of the mansion pyroclast fall succession, St. Kitts. Bull Volcanol 43, 303–310. https://doi.org/10.1007/BF02598034

Baker, P.E., 1969. The geological history of Mt Misery Volcano, St Kitts, West Indies. HM Stationery Office.

Baker, P.E., 1968. Petrology of Mt. Misery Volcano, St. Kitts, West Indies. Lithos 1, 124–150. https://doi.org/10.1016/S0024-4937(68)80004-0

Baker, P.E., Holland, J.G., 1973. Geochemical variations in a pyroclastic succession on St. Kitts, west Indies. Bull Volcanol 37, 472–490. https://doi.org/10.1007/BF02596887

Blundy, J., Cashman, K., 2008. Petrologic Reconstruction of Magmatic System Variables and Processes. Reviews in Mineralogy and Geochemistry 69, 179–239. https://doi.org/10.2138/rmg.2008.69.6

Blundy, J.D., Holland, T.J.B., 1990. Calcic amphibole equilibria and a new amphibole-plagioclase geothermometer. Contr. Mineral. and Petrol. 104, 208–224. https://doi.org/10.1007/BF00306444

Camejo-Harry, M., Melekhova, E., Blundy, J., Attridge, W., Robertson, R., Christopher, T., 2018. Magma evolution beneath Bequia, Lesser Antilles, deduced from petrology of lavas and plutonic xenoliths. Contrib Mineral Petrol 173, 77. https://doi.org/10.1007/s00410-018-1504-z

Caricchi, L., 2013. Frequency and magnitude of volcanic eruptions controlled by magma injection and buoyancy. NATURE GEOSCIENCE 6.

Caricchi, L., Blundy, J., 2015. Experimental petrology of monotonous intermediate magmas. Geological Society, London, Special Publications 422, 105–130.

Cashman, K., Biggs, J., 2014. Common processes at unique volcanoes—a volcanological conundrum. Front. Earth Sci. 2. https://doi.org/10.3389/feart.2014.00028

Cashman, K., Blundy, J., 2013. Petrological cannibalism: the chemical and textural consequences of incremental magma body growth. Contrib Mineral Petrol 166, 703–729. https://doi.org/10.1007/s00410-013-0895-0

Cashman, K.V., Sparks, R.S.J., Blundy, J.D., 2017. Vertically extensive and unstable magmatic systems: A unified view of igneous processes. Science 355, eaag3055. https://doi.org/10.1126/science.aag3055

Christopher, T.E., Blundy, J., Cashman, K., Cole, P., Edmonds, M., Smith, P.J., Sparks, R.S.J., Stinton, A., 2015. Crustal-scale degassing due to magma system destabilization and magma-gas decoupling at

Soufrière Hills Volcano, Montserrat. Geochemistry, Geophysics, Geosystems 16, 2797–2811. https://doi.org/10.1002/2015GC005791

Cooper, G.F., Davidson, J.P., Blundy, J.D., 2016. Plutonic xenoliths from Martinique, Lesser Antilles: evidence for open system processes and reactive melt flow in island arc crust. Contributions to Mineralogy and Petrology 171, 87.

Cooper, G.F., Macpherson, C.G., Blundy, J.D., Maunder, B., Allen, R.W., Goes, S., Collier, J.S., Bie, L., Harmon, N., Hicks, S.P., Iveson, A.A., Prytulak, J., Rietbrock, A., Rychert, C.A., Davidson, J.P., 2020. Variable water input controls evolution of the Lesser Antilles volcanic arc. Nature 582, 525–529. https://doi.org/10.1038/s41586-020-2407-5

Danyushevsky, L.V., Falloon, T.J., Sobolev, A.V., Crawford, A.J., Carroll, M., Price, R.C., 1993. The H_2O content of basalt glasses from Southwest Pacific back-arc basins. Earth and Planetary Science Letters 117, 347–362. https://doi.org/10.1016/0012-821X(93)90089-R

Davidson, J., Turner, S., Handley, H., Macpherson, C., Dosseto, A., 2007. Amphibole “sponge” in arc crust? Geology 35, 787–790. https://doi.org/10.1130/G23637A.1

Davidson, J.P., Boghossian, N.D., Wilson, M., 1993. The Geochemistry of the Igneous Rock Suite of St Martin, Northern Lesser Antilles. J Petrology 34, 839–866. https://doi.org/10.1093/petrology/34.5.839

Deer, W.A., Howie, R.A., Zussman, J., 1997. Rock-Forming Minerals: Disilicates and Ring Silicates, Volume 1B. Geological Society of London.

Dyar, M.D., Mackwell, S.J., McGuire, A.V., Cross, L.R., Robertson, J.D., 1993. Crystal chemistry of Fe^{3+} and H^+ in mantle kaersutite: Implications for mantle metasomatism. American Mineralogist 78, 968–979.

Dyar, M.D., McGuire, A.V., Mackwell, S.J., 1992. Fe^{3+}/H^+ and D/H in kaersutites—Misleading indicators of mantle source fugacities. Geology 20, 565–568. https://doi.org/10.1130/0091-7613(1992)020<0565:FHADHI>2.3.CO;2

Edmonds, M., Humphreys, M.C.S., Hauri, E.H., Herd, R.A., Wadge, G., Rawson, H., Ledden, R., Plail, M., Barclay, J., Aiuppa, A., Christopher, T.E., Giudice, G., Guida, R., 2014. Chapter 16 Pre-eruptive vapour and its role in controlling eruption style and longevity at Soufrière Hills Volcano. Geological Society, London, Memoirs 39, 291–315. https://doi.org/10.1144/M39.16

Edmonds, M., Kohn, S.C., Hauri, E.H., Humphreys, M.C.S., Cassidy, M., 2016. Extensive, water-rich magma reservoir beneath southern Montserrat. Lithos 252–253, 216–233. https://doi.org/10.1016/j.lithos.2016.02.026

Erdmann, S., Martel, C., Pichavant, M., Kushnir, A., 2014. Amphibole as an archivist of magmatic crystallization conditions: problems, potential, and implications for inferring magma storage prior to the paroxysmal 2010 eruption of Mount Merapi, Indonesia. Contributions to Mineralogy and Petrology 6, 1–23. https://doi.org/10.1007/s00410-014-1016-4

Faure, F., Schiano, P., 2005. Experimental investigation of equilibration conditions during forsterite growth and melt inclusion formation. Earth and Planetary Science Letters 236, 882–898. https://doi.org/10.1016/j.epsl.2005.04.050

Foden, J.D., Green, D.H., 1992. Possible role of amphibole in the origin of andesite: some experimental and natural evidence. Contr. Mineral. and Petrol. 109, 479–493. https://doi.org/10.1007/BF00306551

Gertisser, R., Keller, J., 2003. Temporal variations in magma composition at Merapi Volcano (Central Java, Indonesia): magmatic cycles during the past 2000 years of explosive activity. Journal of Volcanology and Geothermal Research, Volcanic hazards: Monitoring, prediction and mitigation 123, 1–23. https://doi.org/10.1016/S0377-0273(03)00025-8

Ghiorso, M.S., Gualda, G.A., 2015. An H2O–CO2 mixed fluid saturation model compatible with rhyolite-MELTS. Contributions to Mineralogy and Petrology 169, 53.

Giordano, D., Russell, J.K., Dingwell, D.B., 2008. Viscosity of magmatic liquids: A model. Earth and Planetary Science Letters 271, 123–134. https://doi.org/10.1016/j.epsl.2008.03.038

Grove, T.L., Baker, M.B., Kinzler, R.J., 1984. Coupled CaAl-NaSi diffusion in plagioclase feldspar: Experiments and applications to cooling rate speedometry. Geochimica et Cosmochimica Acta 48, 2113–2121. https://doi.org/10.1016/0016-7037(84)90391-0

Grove, T.L., Till, C.B., Krawczynski, M.J., 2012. The Role of H2O in Subduction Zone Magmatism. Annual Review of Earth and Planetary Sciences 40, 413–439. https://doi.org/10.1146/annurev-earth-042711-105310

Hammer, J., Jacob, S., Welsch, B., Hellebrand, E., Sinton, J., 2016. Clinopyroxene in postshield Haleakala ankaramite: 1. Efficacy of thermobarometry. Contrib Mineral Petrol 171, 7. https://doi.org/10.1007/s00410-015-1212-x

Harkness, D.D., Roobol, M.J., Smith, A.L., Stipp, J.J., Baker, P.E., 1994. Radiocarbon redating of contaminated samples from a tropical volcano: the Mansion ‘Series’ of St Kitts, West Indies. Bull Volcanol 56, 326–334. https://doi.org/10.1007/BF00326459

Hauri, E.H., Gaetani, G.A., Green, T.H., 2006. Partitioning of water during melting of the Earth's upper mantle at H2O-undersaturated conditions. Earth and Planetary Science Letters 248, 715–734. https://doi.org/10.1016/j.epsl.2006.06.014

Hawthorne, F., Oberti, R., 2007. Amphiboles: Crystal Chemistry. Reviews in Mineralogy and Geochemistry 67, 1–54. https://doi.org/10.2138/rmg.2007.67.1

Hervig, R.L., Dunbar, N., Westrich, H.R., Kyle, P.R., 1989. Pre-eruptive water content of rhyolitic magmas as determined by ion microprobe analyses of melt inclusions in phenocrysts. Journal of Volcanology and Geothermal Research 36, 293–302. https://doi.org/10.1016/0377-0273(89)90075-9

Higgins. 0., Sheldrake. T., Caricchi. L., 2021. Quantitative chemical mapping of plagioclase as a tool for the interpretation of volcanic stratigraphy: an example from Saint Kitts (Lesser Antilles). Bulletin of Volcanology (accepted)

Hildreth, W., Moorbath, S., 1988. Crustal contributions to arc magmatism in the Andes of central Chile. Contributions to mineralogy and petrology 98, 455–489.

Hirschmann, M.M., Ghiorso, M.S., Davis, F.A., Gordon, S.M., Mukherjee, S., Grove, T.L., Krawczynski, M., Medard, E., Till, C.B., 2008. Library of Experimental Phase Relations (LEPR): A database and Web portal for experimental magmatic phase equilibria data. Geochemistry, Geophysics, Geosystems 9. https://doi.org/10.1029/2007GC001894

Holland, T., Blundy, J., 1994. Non-ideal interactions in calcic amphiboles and their bearing on amphibole-plagioclase thermometry. Contr. Mineral. and Petrol. 116, 433–447. https://doi.org/10.1007/BF00310910

Howe, T.M., Lindsay, J.M., Shane, P., Schmitt, A.K., Stockli, D.F., 2014. Re-evaluation of the Roseau Tuff eruptive sequence and other ignimbrites in Dominica, Lesser Antilles. Journal of Quaternary Science 29, 531–546. https://doi.org/10.1002/jqs.2723

Jackson, M.D., Blundy, J., Sparks, R.S.J., 2018. Chemical differentiation, cold storage and remobilization of magma in the Earth's crust. Nature 564, 405–409. https://doi.org/10.1038/s41586-018-0746-2

Karakas, O., Degruyter, W., Bachmann, O., Dufek, J., 2017. Lifetime and size of shallow magma bodies controlled by crustal-scale magmatism. Nature Geosci 10, 446–450. https://doi.org/10.1038/ngeo2959

Klaver, M., Blundy, J.D., Vroon, P.Z., 2018. Generation of arc rhyodacites through cumulate-melt reactions in a deep crustal hot zone: Evidence from Nisyros volcano. Earth and Planetary Science Letters 497, 169–180. https://doi.org/10.1016/j.epsl.2018.06.019

Klaver, M., Matveev, S., Berndt, J., Lissenberg, C.J., Vroon, P.Z., 2017. A mineral and cumulate perspective to magma differentiation at Nisyros volcano, Aegean arc. Contrib Mineral Petrol 172, 95. https://doi.org/10.1007/s00410-017-1414-5

Kopp, H., Weinzierl, W., Becel, A., Charvis, P., Evain, M., Flueh, E.R., Gailler, A., Galve, A., Hirn, A., Kandilarov, A., Klaeschen, D., Laigle, M., Papenberg, C., Planert, L., Roux, E., 2011. Deep structure of the central Lesser Antilles Island Arc: Relevance for the formation of continental crust. Earth and Planetary Science Letters 304, 121–134. https://doi.org/10.1016/j.epsl.2011.01.024

Leake, B.E., Woolley, A.R., Arps, C.E., Birch, W.D., Gilbert, M.C., Grice, J.D., Hawthorne, F.C., Kato, A., Kisch, H.J., Krivovichev, V.G., 1997. Report. Nomenclature of amphiboles: report of the subcommittee on amphiboles of the international mineralogical association commission on new minerals and mineral names. Mineralogical magazine 61, 295–321.

Lindsay, J.M., 2005. Volcanic hazard atlas of the Lesser Antilles. Seismic Research.

Marsh, B.D., 1981. On the crystallinity, probability of occurrence, and rheology of lava and magma. Contr. Mineral. and Petrol. 78, 85–98. https://doi.org/10.1007/BF00371146

Martel, C., Champallier, R., Prouteau, G., Pichavant, M., Arbaret, L., Balcone-Boissard, H., Boudon, G., Boivin, P., Bourdier, J.-L., Scaillet, B., 2013. Trachyte Phase Relations and Implication for Magma Storage Conditions in the Chaine des Puys (French Massif Central). Journal of Petrology 54, 1071–1107. https://doi.org/10.1093/petrology/egt006

Marxer, F., Ulmer, P., 2019. Crystallisation and zircon saturation of calc-alkaline tonalite from the Adamello Batholith at upper crustal conditions: an experimental study. Contrib Mineral Petrol 174, 84. https://doi.org/10.1007/s00410-019-1619-x

Melekhova, E., Blundy, J., Martin, R., Arculus, R., Pichavant, M., 2017. Petrological and experimental evidence for differentiation of water-rich magmas beneath St. Kitts, Lesser Antilles. Contrib Mineral Petrol 172, 98. https://doi.org/10.1007/s00410-017-1416-3

Melekhova, E., Blundy, J., Robertson, R., Humphreys, M.C.S., 2015. Experimental Evidence for Polybaric Differentiation of Primitive Arc Basalt beneath St. Vincent, Lesser Antilles. J Petrology 56, 161–192. https://doi.org/10.1093/petrology/egu074

Melekhova, E., Schlaphorst, D., Blundy, J., Kendall, J.-M., Connolly, C., McCarthy, A., Arculus, R., 2019. Lateral variation in crustal structure along the Lesser Antilles arc from petrology of crustal xenoliths and seismic receiver functions. Earth and Planetary Science Letters 516, 12–24. https://doi.org/10.1016/j.epsl.2019.03.030

Mollo, S., Del Gaudio, P., Ventura, G., Iezzi, G., Scarlato, P., 2010. Dependence of clinopyroxene composition on cooling rate in basaltic magmas: Implications for thermobarometry. Lithos 118, 302–312. https://doi.org/10.1016/j.lithos.2010.05.006

Müntener, O., Ulmer, P., 2018. Arc crust formation and differentiation constrained by experimental petrology. Am J Sci 318, 64–89. https://doi.org/10.2475/01.2018.04

Nakamura, M., Shimakita, S., 1998. Dissolution origin and syn-entrapment compositional change of melt inclusion in plagioclase. Earth and Planetary Science Letters 161, 119–133. https://doi.org/10.1016/S0012-821X(98)00144-7

Nandedkar, R.H., Ulmer, P., Müntener, O., 2014. Fractional crystallization of primitive, hydrous arc magmas: an experimental study at 0.7 GPa. Contributions to Mineralogy and Petrology 167, 1015.

Neave, D.A., Bali, E., Guðfinnsson, G.H., Halldórsson, S.A., Kahl, M., Schmidt, A.-S., Holtz, F., 2019. Clinopyroxene–Liquid Equilibria and Geothermobarometry in Natural and Experimental Tholeiites: the 2014–2015 Holuhraun Eruption, Iceland. Journal of Petrology 60, 1653–1680. https://doi.org/10.1093/petrology/egz042

Neave, D.A., Putirka, K.D., 2017. A new clinopyroxene-liquid barometer, and implications for magma storage pressures under Icelandic rift zones. American Mineralogist 102, 777–794.

Nimis, P., 1995. A clinopyroxene geobarometer for basaltic systems based on crystal-structure modeling. Contributions to Mineralogy and Petrology 121, 115–125.

Nimis, P., Ulmer, P., 1998. Clinopyroxene geobarometry of magmatic rocks Part 1: An expanded structural geobarometer for anhydrous and hydrous, basic and ultrabasic systems. Contributions to Mineralogy and Petrology 133, 122–135.

Perinelli, C., Mollo, S., Gaeta, M., Cristofaro, S.P.D., Palladino, D.M., Armienti, P., Scarlato, P., Putirka, K.D., 2016. An improved clinopyroxene-based hygrometer for Etnean magmas and implications for eruption triggering mechanisms. American Mineralogist 101, 2774–2777. https://doi.org/10.2138/am-2016-5916

Petrelli, M., Caricchi, L., Perugini, D., 2020. Machine Learning Thermo-Barometry: Application to Clinopyroxene-Bearing Magmas. Journal of Geophysical Research: Solid Earth 125, e2020JB020130. https://doi.org/10.1029/2020JB020130

Pichavant, M., Costa, F., Burgisser, A., Scaillet, B., Martel, C., Poussineau, S., 2007. Equilibration Scales in Silicic to Intermediate Magmas Implications for Experimental Studies. Journal of Petrology 48, 1955–1972. https://doi.org/10.1093/petrology/egm045

Pichavant, M., Macdonald, R., 2007. Crystallization of primitive basaltic magmas at crustal pressures and genesis of the calc-alkaline igneous suite: experimental evidence from St Vincent, Lesser Antilles arc. Contributions to Mineralogy and Petrology 154, 535–558.

Pichavant, M., Martel, C., Bourdier, J.-L., Scaillet, B., 2002. Physical conditions, structure, and dynamics of a zoned magma chamber: Mount Pelée (Martinique, Lesser Antilles Arc). Journal of Geophysical Research: Solid Earth 107, ECV 1-1-ECV 1-28. https://doi.org/10.1029/2001JB000315

Plank, T., Kelley, K.A., Zimmer, M.M., Hauri, E.H., Wallace, P.J., 2013. Why do mafic arc magmas contain ∼4wt% water on average? Earth and Planetary Science Letters 364, 168–179. https://doi.org/10.1016/j.epsl.2012.11.044

Putirka, K., 2016. Amphibole thermometers and barometers for igneous systems and some implications for eruption mechanisms of felsic magmas at arc volcanoes. American Mineralogist 101, 841–858. https://doi.org/10.2138/am-2016-5506

Putirka, K.D., 2008. Thermometers and Barometers for Volcanic Systems. Reviews in Mineralogy and Geochemistry 69, 61–120. https://doi.org/10.2138/rmg.2008.69.3

Reubi, O., Blundy, J., 2009. A dearth of intermediate melts at subduction zone volcanoes and the petrogenesis of arc andesites. Nature 461, 1269–1273. https://doi.org/10.1038/nature08510

Ridolfi, F., Puerini, M., Renzulli, A., Menna, M., Toulkeridis, T., 2008. The magmatic feeding system of El Reventador volcano (Sub-Andean zone, Ecuador) constrained by texture, mineralogy and thermobarometry of the 2002 erupted products. Journal of Volcanology and Geothermal Research 176, 94–106.

Ridolfi, F., Renzulli, A., 2012. Calcic amphiboles in calc-alkaline and alkaline magmas: thermobarometric and chemometric empirical equations valid up to 1,130° C and 2.2 GPa. Contributions to Mineralogy and Petrology 163, 877–895.

Ridolfi, F., Renzulli, A., Puerini, M., 2010. Stability and chemical equilibrium of amphibole in calc-alkaline magmas: an overview, new thermobarometric formulations and application to subduction-related volcanoes. Contributions to Mineralogy and Petrology 160, 45–66.

Roobol, M.J., Smith, A.L., Wright, J.V., 1985. Dispersal and characteristics of pyroclastic fall deposits from Mt. Misery Volcano, West Indies. Geol Rundsch 74, 321–335. https://doi.org/10.1007/BF01824899

Roobol, M.J., Smith, A.L., Wright, J.V., 1981. Revisions in the pyroclastic stratigraphy of Mt Misery volcano, St. Kitts, Lesser Antilles: 14C ages and recognition of pyroclastic flow deposits. Journal of the Geological Society 138, 713–718.

Scaillet, B., Evans, B.W., 1999. The 15 June 1991 Eruption of Mount Pinatubo. I. Phase Equilibria and Pre-eruption P–T–fO2–fH2O Conditions of the Dacite Magma. Journal of Petrology 40, 381–411. https://doi.org/10.1093/petroj/40.3.381

Shane, P., 2013. Using amphibole crystals to reconstruct magma storage temperatures and pressures for the post-caldera collapse volcanism at Okataina volcano 12.

Sheldrake, T., Higgins, O., 2021, Classification, segmentation and correlation of zoned minerals, Computers & Geosciences (accepted)

Shepherd, J.B., 1984. Segmentation of the Lesser Antilles subduction zone. Earth and Planetary Science Letters 71, 297–304. https://doi.org/10.1016/0012-821X(84)90094-3

Simm, J., Abril, I.M.D., Sugiyama, M., 2014. Tree-Based Ensemble Multi-Task Learning Method for Classification and Regression. IEICE TRANSACTIONS on Information and Systems E97-D, 1677–1681.

Sisson, T.W., Grove, T.L., 1993. Experimental investigations of the role of H2O in calc-alkaline differentiation and subduction zone magmatism. Contr. Mineral. and Petrol. 113, 143–166. https://doi.org/10.1007/BF00283225

Sisson, T.W., Ratajeski, K., Hankins, W.B., Glazner, A.F., 2005. Voluminous granitic magmas from common basaltic sources. Contributions to Mineralogy and Petrology 148, 635–661.

Sisson, T.W., Vallance, J.W., 2009. Frequent eruptions of Mount Rainier over the last ∼2,600 years. Bull Volcanol 71, 595–618. https://doi.org/10.1007/s00445-008-0245-7

Smith, D.J., 2014. Clinopyroxene precursors to amphibole sponge in arc crust. Nature Communications 5, 4329. https://doi.org/10.1038/ncomms5329

Solaro, C., Martel, C., Champallier, R., Boudon, G., Balcone-Boissard, H., Pichavant, M., 2019. Petrological and experimental constraints on magma storage for large pumiceous eruptions in Dominica island (Lesser Antilles). Bull Volcanol 81, 55. https://doi.org/10.1007/s00445-019-1313-x

Sparks, R.S.J., Annen, C., Blundy, J.D., Cashman, K.V., Rust, A.C., Jackson, M.D., 2019. Formation and dynamics of magma reservoirs. Phil. Trans. R. Soc. A. 377, 20180019. https://doi.org/10.1098/rsta.2018.0019

Stamper, C.C., Blundy, J.D., Arculus, R.J., Melekhova, E., 2014. Petrology of Plutonic Xenoliths and Volcanic Rocks from Grenada, Lesser Antilles. Journal of Petrology 55, 1353–1387. https://doi.org/10.1093/petrology/egu027

Stock, M.J., Geist, D., Neave, D.A., Gleeson, M.L.M., Bernard, B., Howard, K.A., Buisman, I., Maclennan, J., 2020. Cryptic evolved melts beneath monotonous basaltic shield volcanoes in the Galápagos Archipelago. Nature Communications 11, 3767. https://doi.org/10.1038/s41467-020-17590-x

Stolper, E., Walker, D., 1980. Melt density and the average composition of basalt. Contr. Mineral. and Petrol. 74, 7–12. https://doi.org/10.1007/BF00375484

Tate, M.P., Wilson, M., 1988. Emplacement mechanism and lateral correlation of pyroclastic flow and surge deposits in northen St Kitts, Lesser Antilles. Journal of the Geological Society 145, 553–562. https://doi.org/10.1144/gsjgs.145.4.0553

Team, R.C., 2013. R: A language and environment for statistical computing.

Toothill, J., Williams, C.A., MacDonald, R., Turner, S.P., Rogers, N.W., Hawkesworth, C.J., Jerram, D.A., Ottley, C.J., Tindle, A.G., 2007. A Complex Petrogenesis for an Arc Magmatic Suite, St Kitts, Lesser Antilles. Journal of Petrology 48, 3–42. https://doi.org/10.1093/petrology/egl052

Villiger, S., Ulmer, P., Müntener, O., 2007. Equilibrium and Fractional Crystallization Experiments at 0·7 GPa; the Effect of Pressure on Phase Relations and Liquid Compositions of Tholeiitic Magmas. J Petrology 48, 159–184. https://doi.org/10.1093/petrology/egl058

Voight, B., 1988. A method for prediction of volcanic eruptions 6.

Wadge, G., Shepherd, J.B., 1984. Segmentation of the Lesser Antilles subduction zone. Earth and Planetary Science Letters 71, 297–304. https://doi.org/10.1016/0012-821X(84)90094-3

Waters, L.E., Lange, R.A., 2015. An updated calibration of the plagioclase-liquid hygrometer-thermometer applicable to basalts through rhyolites. American Mineralogist 100, 2172–2184. https://doi.org/10.2138/am-2015-5232

Zajacz, Z., Halter, W., Malfait, W.J., Bachmann, O., Bodnar, R.J., Hirschmann, M.M., Mandeville, C.W., Morizet, Y., Müntener, O., Ulmer, P., Webster, J.D., 2005. A composition-independent quantitative determination of the water content in silicate glasses and silicate melt inclusions by confocal Raman spectroscopy. Contrib Mineral Petrol 150, 631–642. https://doi.org/10.1007/s00410-005-0040-9

Zhang, J., Humphreys, M.C.S., Cooper, G.F., Davidson, J.P., Macpherson, C.G., 2017. Magma mush chemistry at subduction zones, revealed by new melt major element inversion from calcic amphiboles. American Mineralogist 102, 1353–1367. https://doi.org/10.2138/am-2017-5928

Zhang, Y., Xu, Z., Zhu, M., Wang, H., 2007. Silicate melt properties and volcanic eruptions. Reviews of Geophysics 45. https://doi.org/10.1029/2006RG000216

Ziberna, L., Green, E.C.R., Blundy, J.D., 2017. Multiple-reaction geobarometry for olivine-bearing igneous rocks. American Mineralogist 102, 2349–2366. https://doi.org/10.2138/am-2017-6154

Figures

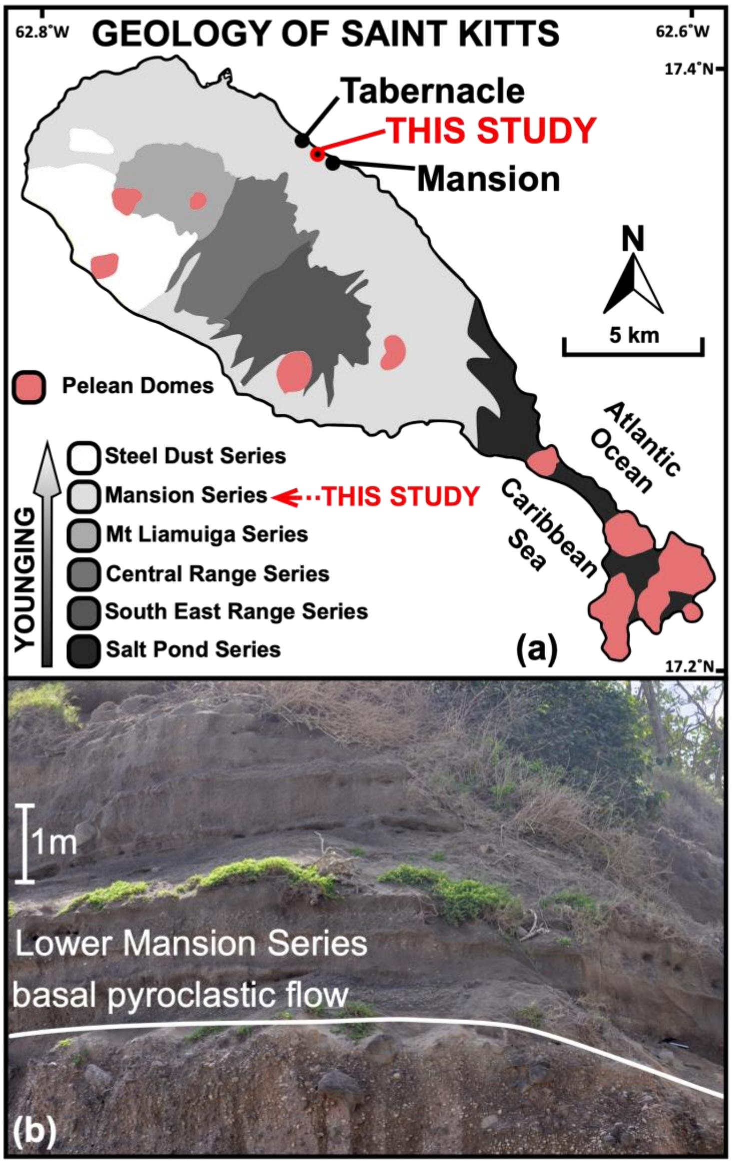

Figure 1

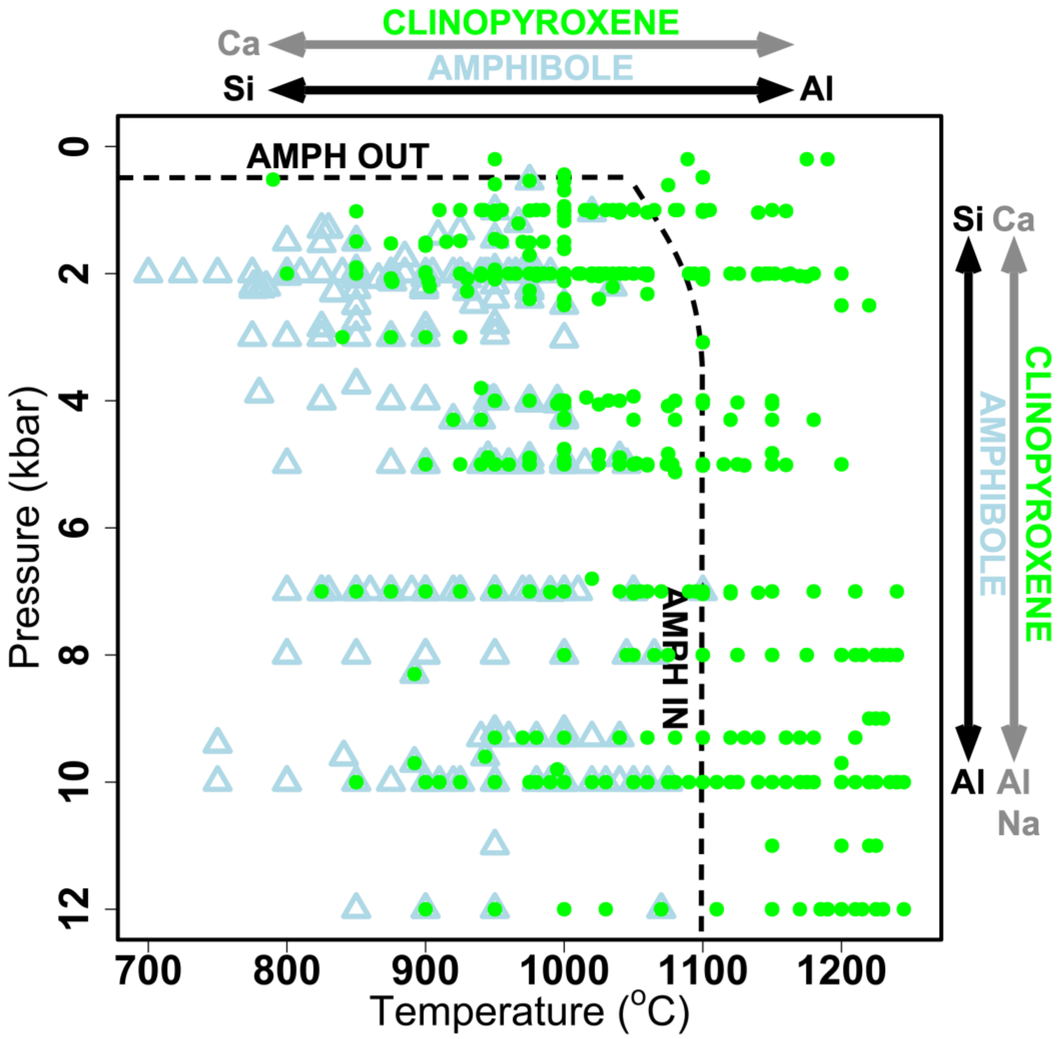
CLINOPYROXENE
Ca
AMPHIBOLE
Si
Al
AMPH OUT
AMPH IN
Pressure (kbar)
0
2
4
6
8
10
12
700
800
900
1000
1100
1200
Temperature (°C)
Si Ca
AMPHIBOLE
CLINOPYROXENE
Al Al
Na

Figure 2

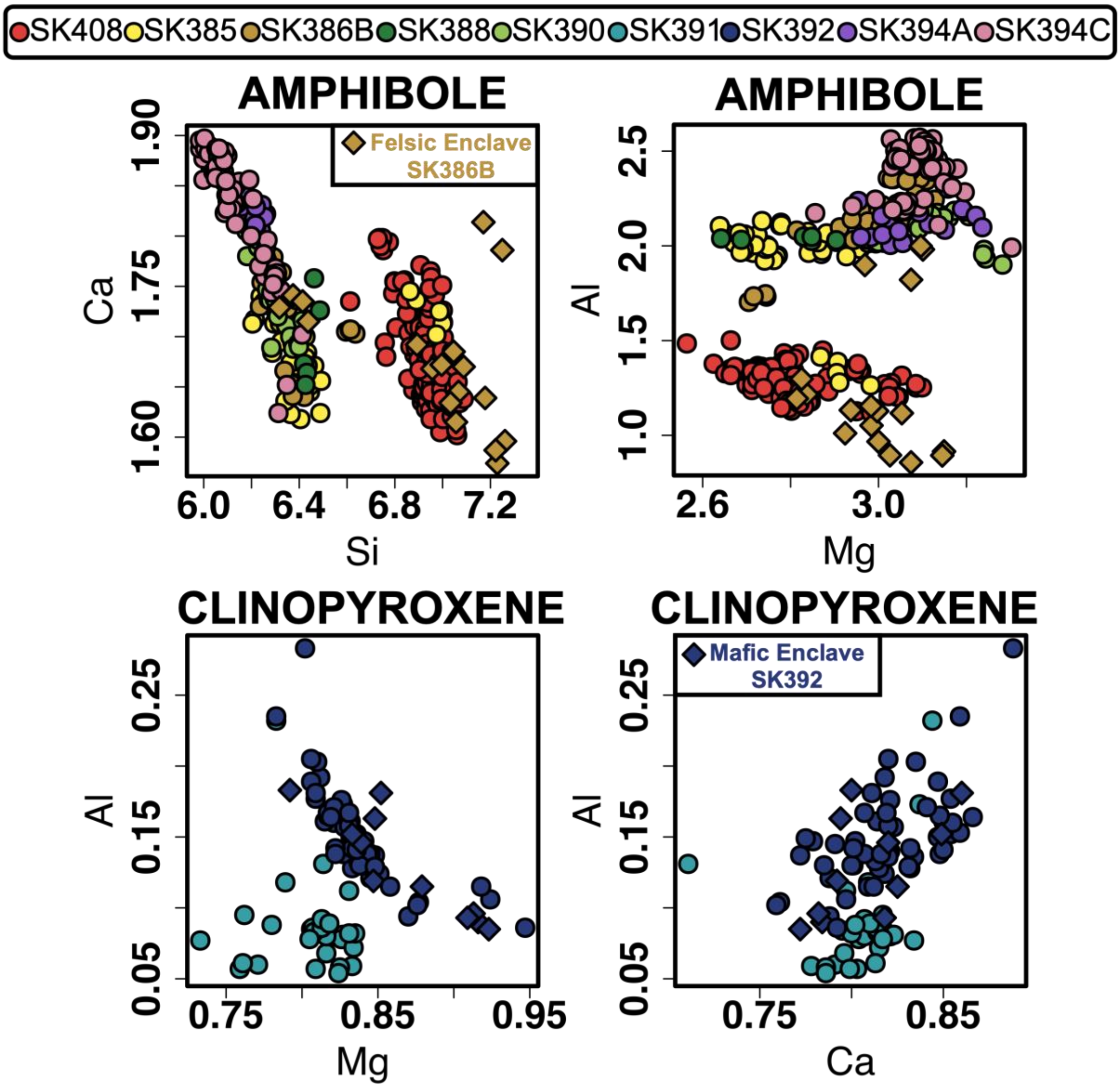
SK408 SK385 SK386B SK388 SK390 SK391 SK392 SK394A SK394C
AMPHIBOLE
Felsic Enclave SK386B
Ca
1.90
1.75
1.60
6.0
6.4
6.8
7.2
Si
AMPHIBOLE
Al
2.5
2.0
1.5
1.0
2.6
3.0
Mg
CLINOPYROXENE
Al
0.25
0.15
0.05
0.75
0.85
0.95
Mg
CLINOPYROXENE
Mafic Enclave SK392
Al
0.25
0.15
0.05
0.75
0.85
Ca

Figure 3

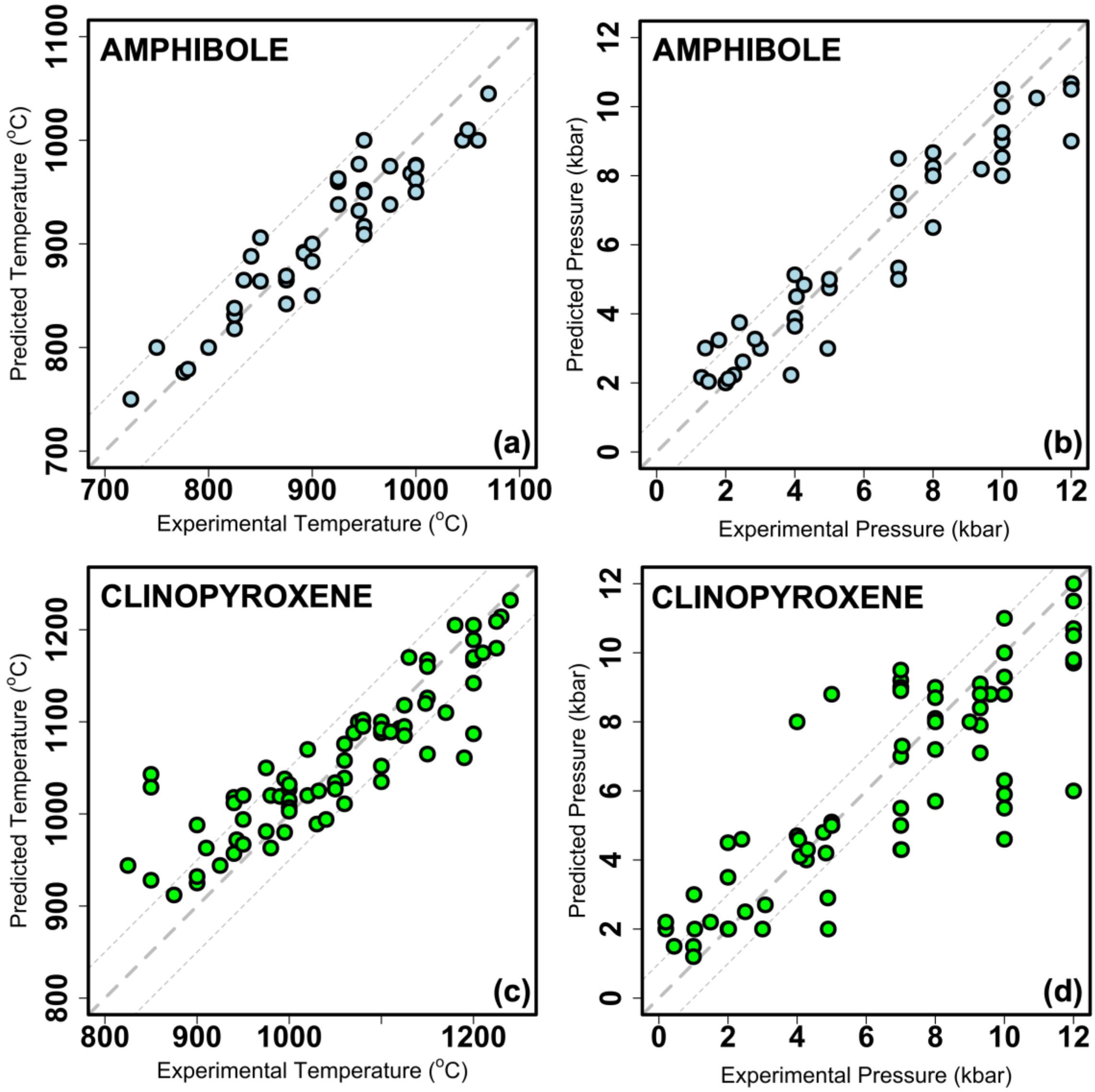
AMPHIBOLE
Predicted Temperature (°C)
Experimental Temperature (°C)
(a)
AMPHIBOLE
Predicted Pressure (kbar)
Experimental Pressure (kbar)
(b)
CLINOPYROXENE
Predicted Temperature (°C)
Experimental Temperature (°C)
(c)
CLINOPYROXENE
Predicted Pressure (kbar)
Experimental Pressure (kbar)
(d)

Figure 4

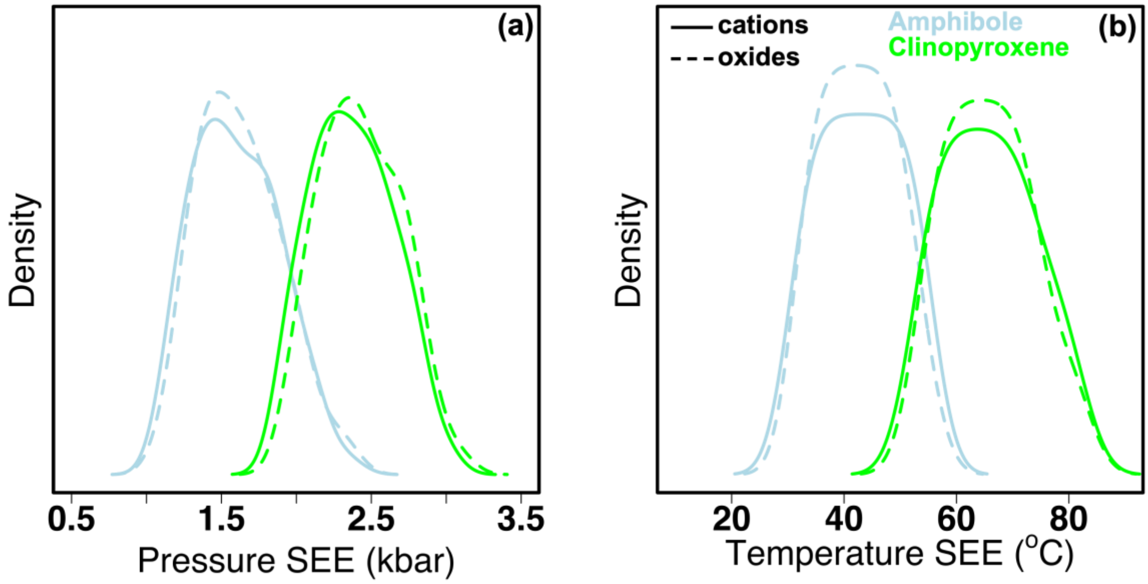
(a)
Density
0.5
1.5
2.5
3.5
Pressure SEE (kbar)
cations
oxides
Amphibole
Clinopyroxene
(b)
Density
20
40
60
80
Temperature SEE (°C)

Figure 5

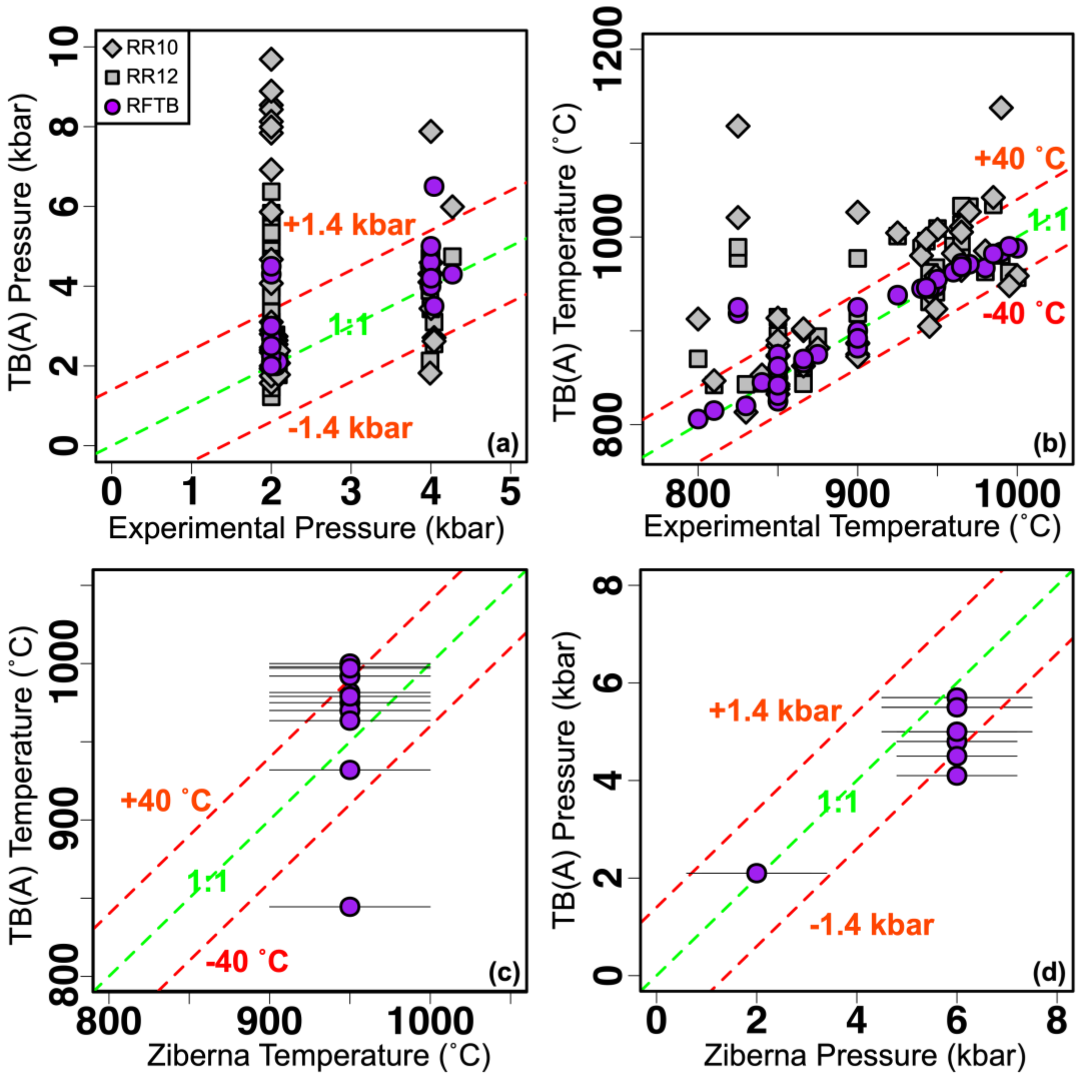

RR10
RR12
RFTB
TB(A) Pressure (kbar)
Experimental Pressure (kbar)
+1.4 kbar
1:1
-1.4 kbar
(a)
TB(A) Temperature (˚C)
Experimental Temperature (˚C)
+40 ˚C
1:1
-40 ˚C
(b)
TB(A) Temperature (˚C)
Ziberna Temperature (˚C)
+40 ˚C
1:1
-40 ˚C
(c)
TB(A) Pressure (kbar)
Ziberna Pressure (kbar)
+1.4 kbar
1:1
-1.4 kbar
(d)

Figure 6

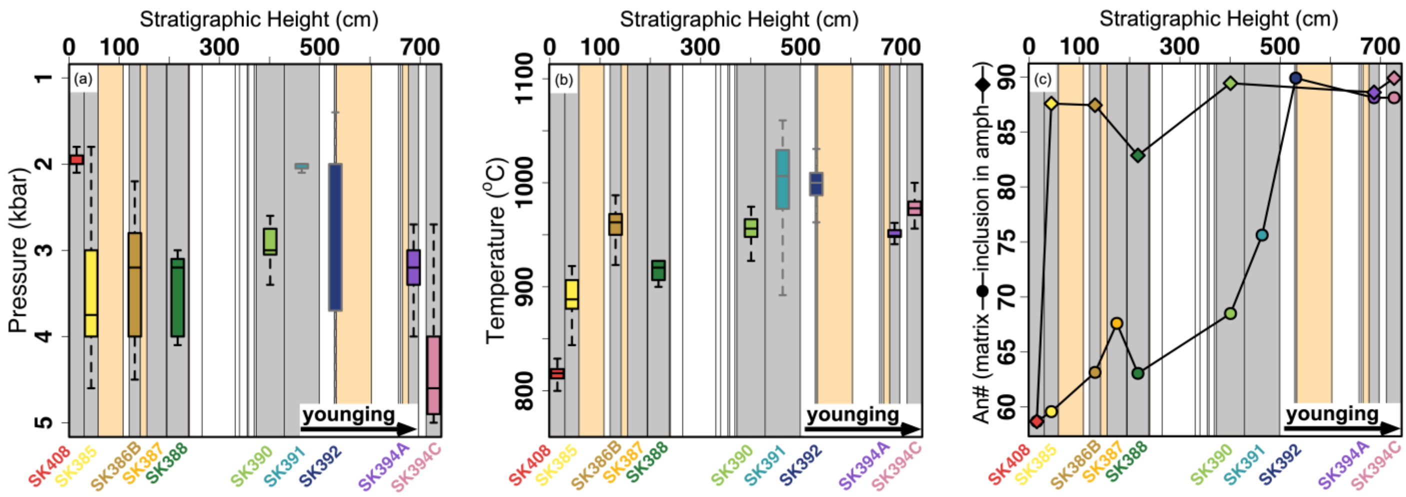
Stratigraphic Height (cm)
(a)
Pressure (kbar)
younging
(b)
Temperature (°C)
(c)
An# (matrix —●— inclusion in amph—◆—)
SK408
SK385
SK386B
SK387
SK388
SK390
SK391
SK392
SK394A
SK394C

Figure 7

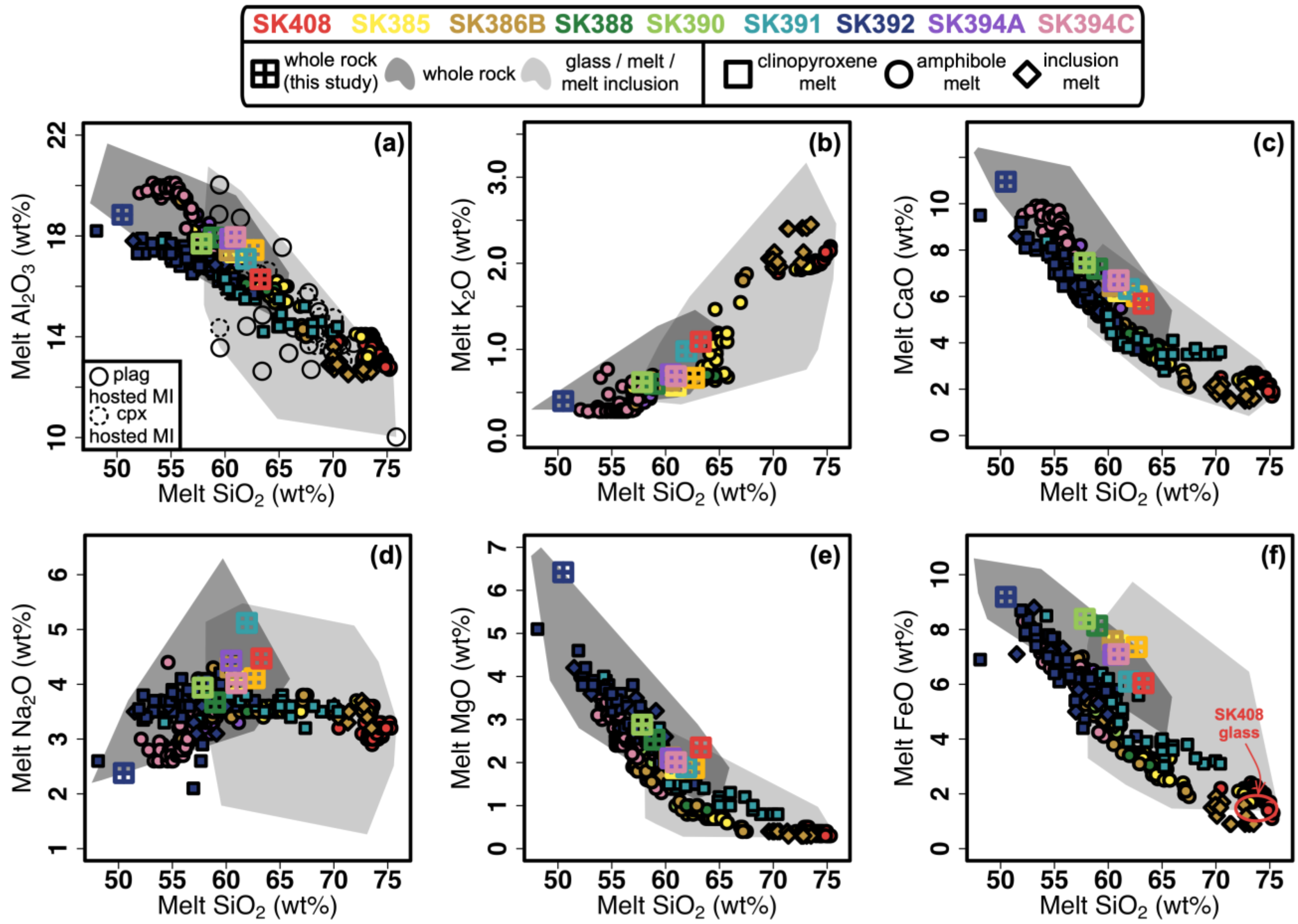
SK408 SK385 SK386B SK388 SK390 SK391 SK392 SK394A SK394C
whole rock (this study)
whole rock
glass / melt / melt inclusion
clinopyroxene melt
amphibole melt
inclusion melt
(a)
(b)
(c)
(d)
(e)
(f)
plag hosted MI
cpx hosted MI
Melt Al2O3 (wt%)
Melt K2O (wt%)
Melt CaO (wt%)
Melt Na2O (wt%)
Melt MgO (wt%)
Melt FeO (wt%)
Melt SiO2 (wt%)
SK408 glass

Figure 8

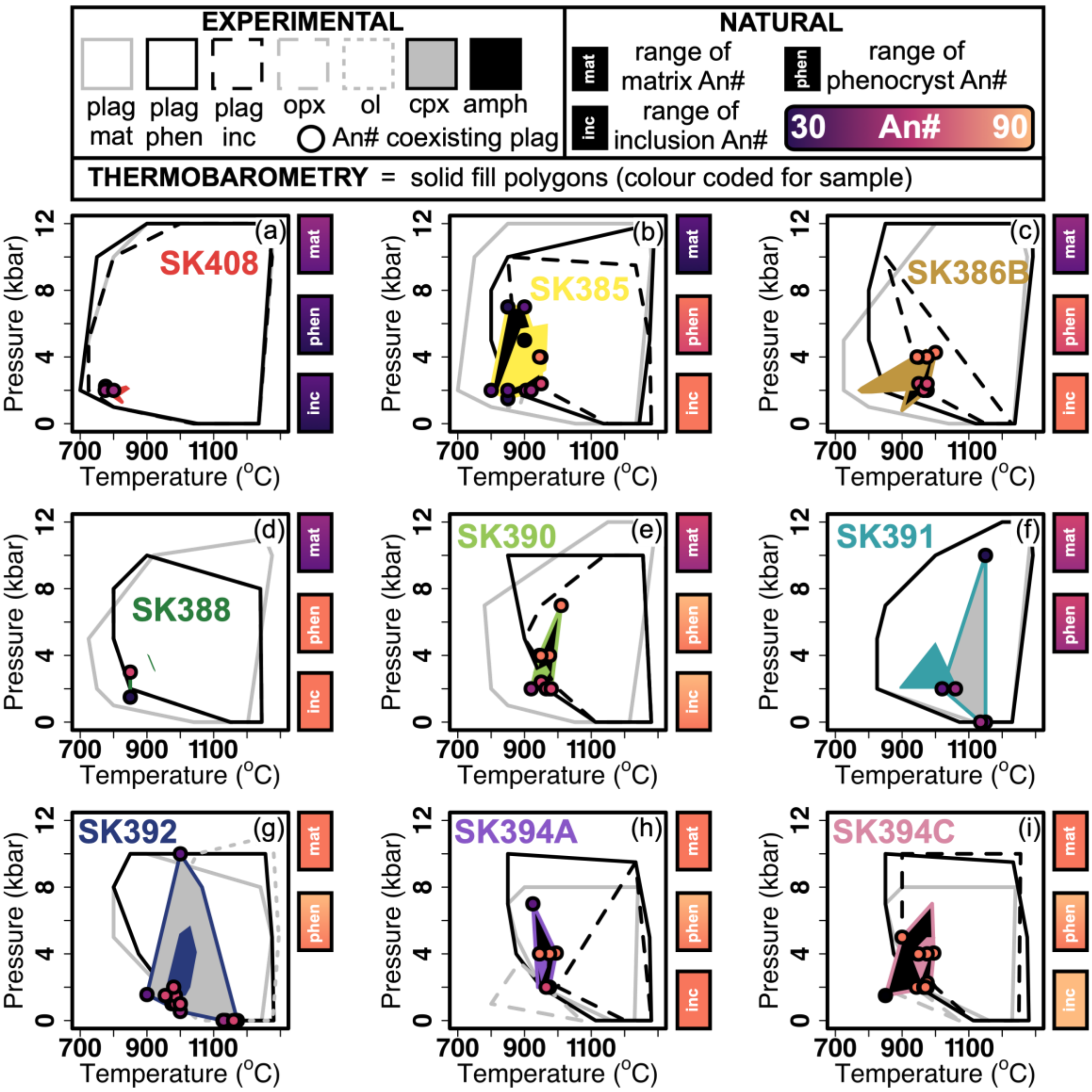
EXPERIMENTAL
plag mat
plag phen
plag inc
opx
ol
cpx
amph
An# coexisting plag
NATURAL
mat range of matrix An#
phen range of phenocryst An#
inc range of inclusion An#
30 An# 90
THERMOBAROMETRY = solid fill polygons (colour coded for sample)
SK408
SK385
SK386B
SK388
SK390
SK391
SK392
SK394A
SK394C
Pressure (kbar)
Temperature (°C)

Figure 9

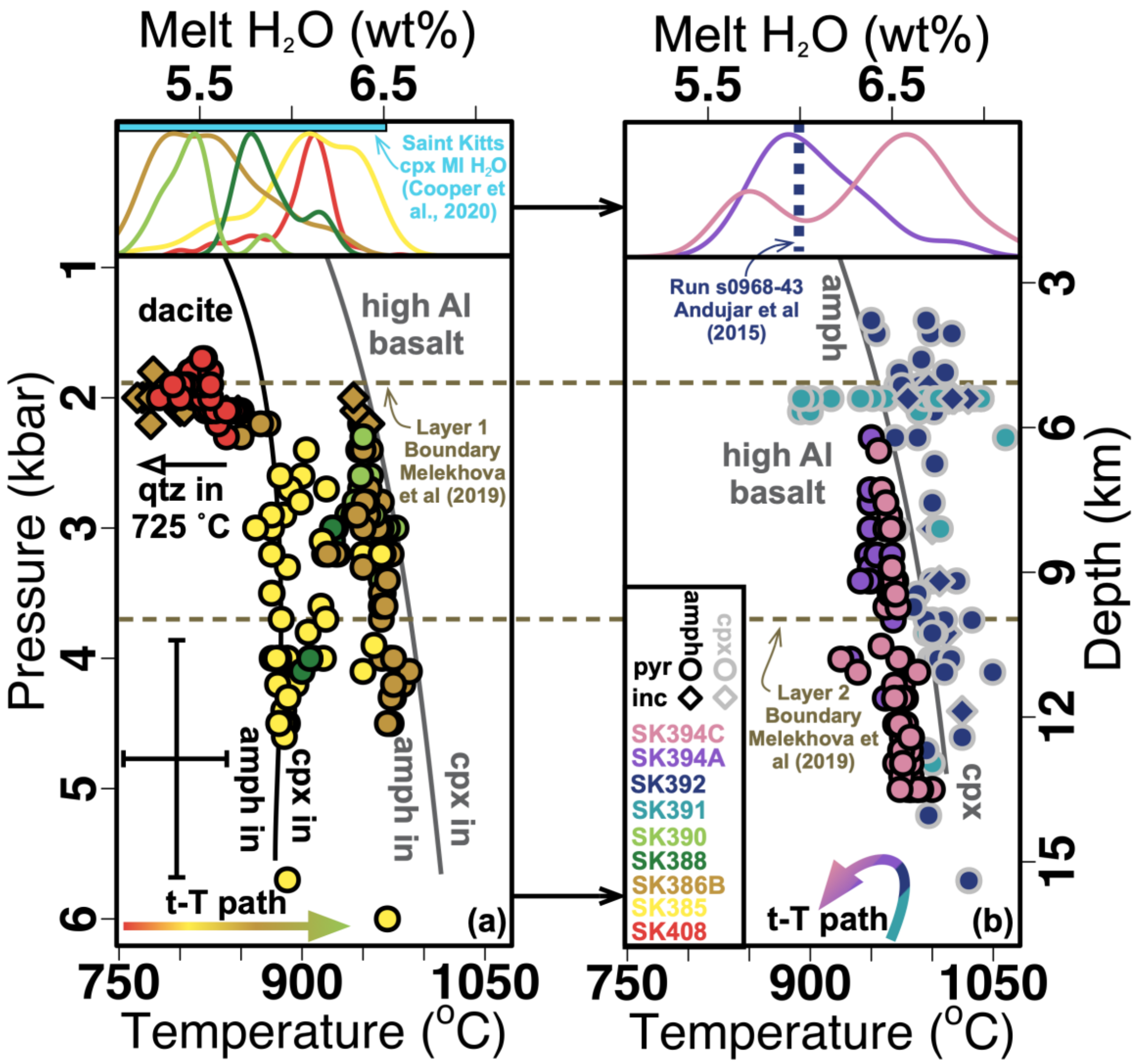

Melt H_2O (wt%)
5.5
6.5
Saint Kitts cpx MI H_2O (Cooper et al., 2020)
dacite
high Al basalt
Layer 1 Boundary Melekhova et al (2019)
qtz in 725 ˚C
amph in
cpx in
t-T path
(a)
Pressure (kbar)
Temperature (°C)
750
900
1050
Run s0968-43 Andujar et al (2015)
amph
cpx
Layer 2 Boundary Melekhova et al (2019)
pyr
inc
SK394C
SK394A
SK392
SK391
SK390
SK388
SK386B
SK385
SK408
(b)
Depth (km)

Figure 10

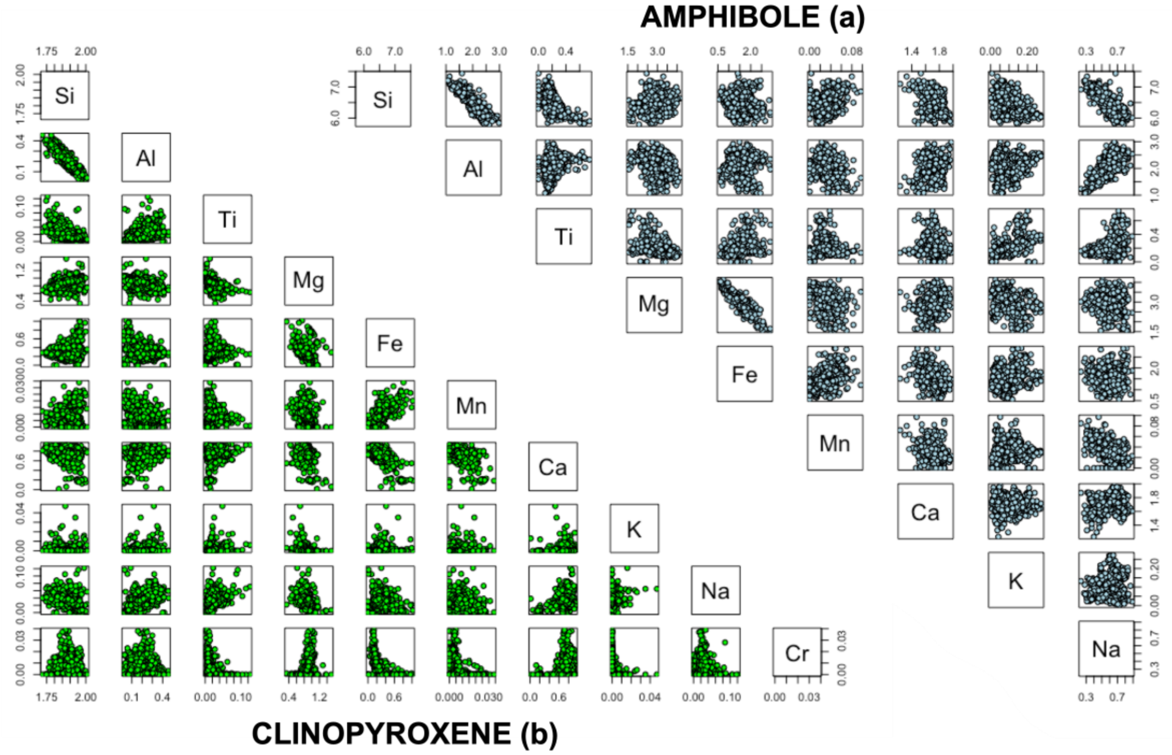

Supplementary Figure 1

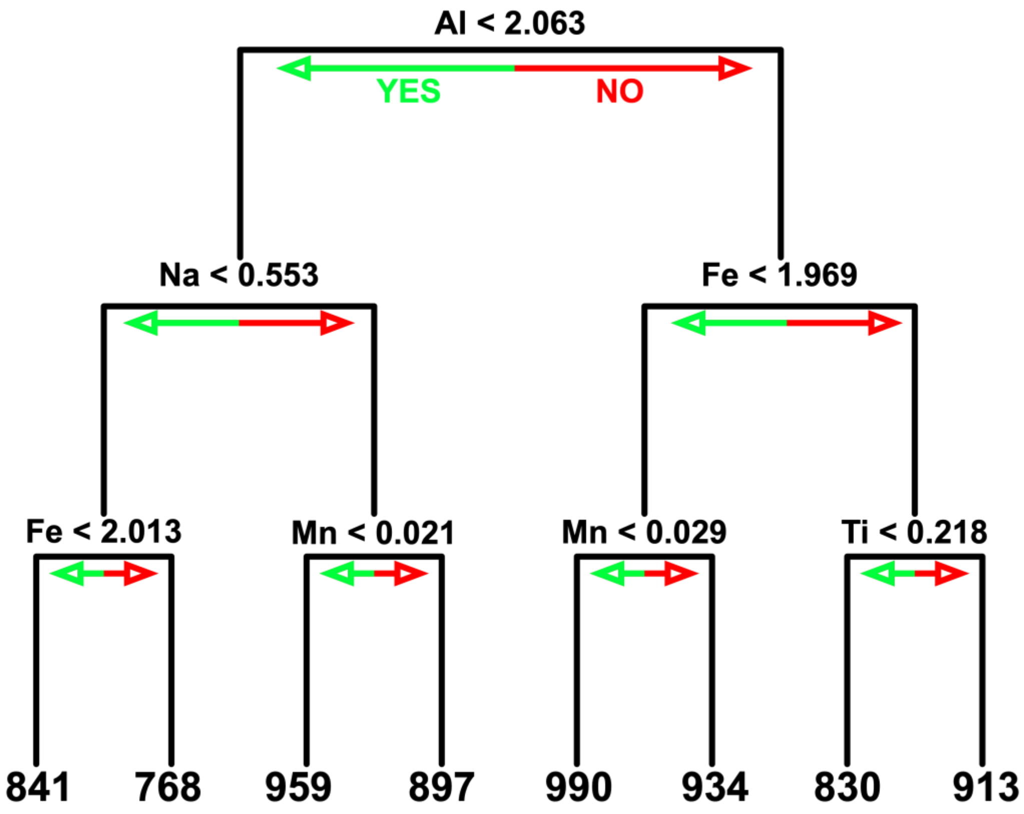

Supplementary Figure 2

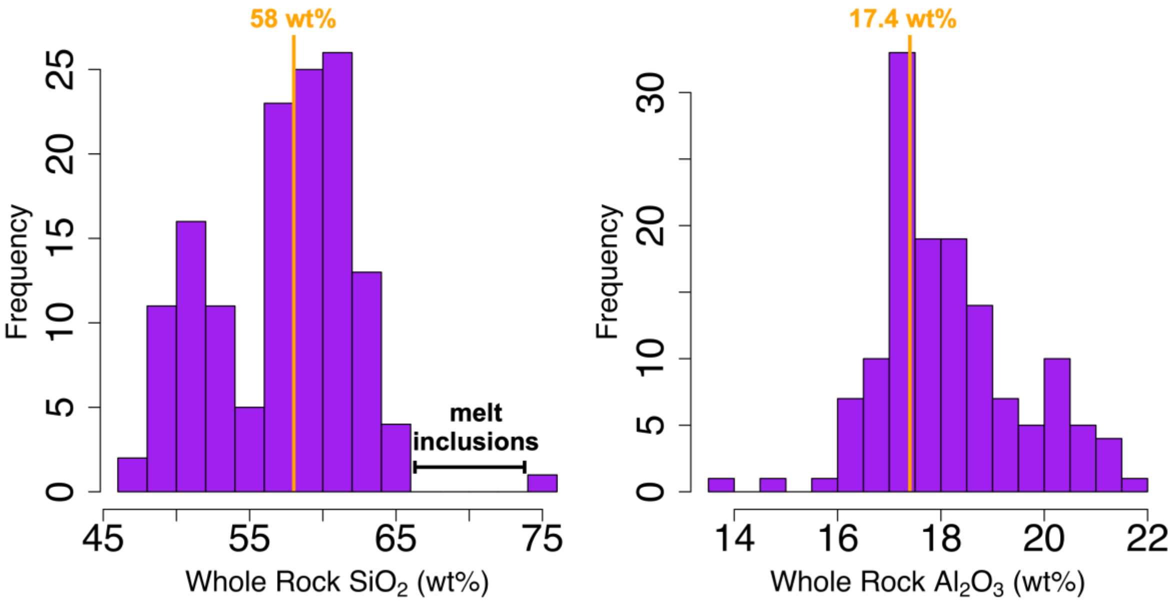

Supplementary Figure 3